World Journal of Gastroenterology

Submit a Manuscript: http://www.f6publishing.com

World J Gastroenterol 2018 April 28; 24(16): 1748-1765

DOI: 10.3748/wjg.v24.i16.1748

ISSN 1007-9327 (print) ISSN 2219-2840 (online)

ORIGINAL ARTICLE

Basic Study

Nonalcoholic steatohepatitis severity is defined by a failure in compensatory antioxidant capacity in the setting of mitochondrial dysfunction

Michelle L Boland, Stephanie Oldham, Brandon B Boland, Sarah Will, Jean-Martin Lapointe, Silvia Guionaud, Christopher J Rhodes, James L Trevaskis

Michelle L Boland, Stephanie Oldham, Brandon B Boland, Sarah Will, Christopher J Rhodes, James L Trevaskis, Cardiovascular and Metabolic Diseases, MedImmune LLC, Gaithersburg, MD 20878, United States

Jean-Martin Lapointe, Pathology, MedImmune Ltd., Cambridge CB21 6GH, United Kingdom

Silvia Guionaud, Pathology, Drug Safety and Metabolism, IMED Biotech Unit, AstraZeneca, Cambridge CB22 3AT, United Kingdom

ORCID number: Michelle L Boland (0000-0002-9920-2088); Stephanie Oldham (0000-0002-0295-1921); Brandon B Boland (0000-0003-1280-9547); Sarah Will (0000-0001-9408-9234); Jean-Martin Lapointe (0000-0003-0141-4603); Silvia Guionaud (0000-0003-1929-6094); Christopher J Rhodes (0000-0002-4852-516X); James L Trevaskis (0000-0002-5356-6118).

Author contributions: Boland ML and Trevaskis JL conceived of the project; Boland ML, Rhodes CJ and Trevaskis JL designed and interpreted experiments; Boland ML, Oldham S, Boland BB, Will S, Lapointe JM and Guionaud S acquired and analyzed data; Boland ML, Boland BB, Rhodes CJ and Trevaskis JL wrote and edited the manuscript.

Supported by MedImmune.

Institutional animal care and use committee statement: All animal experiments were conducted in accordance with policies of the NIH Guide for the Care and Use of Laboratory Animals and the Institutional Animal Care and Use Committee (IACUC) of MedImmune, LLC. Specific protocols used in this study were approved by the MedImmune IACUC, protocol number MI-16-0034.

Conflict-of-interest statement: All authors are current employees and/or stockholders of MedImmune/AstraZeneca.

ARRIVE guidelines statement: The authors have read the ARRIVE guidelines, and the manuscript was prepared and revised according to the ARRIVE guidelines

Manuscript source: Unsolicited manuscript

Correspondence to: James L Trevaskis, PhD, Principal Scientist, Cardiovascular and Metabolic Diseases, MedImmune, LLC, Gaithersburg, MD 20878, United States. trevaskisj@medimmune.com

Telephone: +1-301-3986695

Received: January 17, 2018
Peer-review started: January 17, 2018
First decision: February 11, 2018
Revised: February 22, 2018
Accepted: February 26, 2018
Article in press: February 25, 2018
Published online: April 28, 2018

Abstract

AIM

To comprehensively evaluate mitochondrial (dys) function in preclinical models of nonalcoholic steatohepatitis (NASH).

METHODS

We utilized two readily available mouse models of nonalcoholic fatty liver disease (NAFLD) with or without

progressive fibrosis: *Lep*^{ob}/*Lep*^{ob} (*ob/ob*) and FATZO mice on high *trans*-fat, high fructose and high cholesterol (AMLN) diet. Presence of NASH was assessed using immunohistochemical and pathological techniques, and gene expression profiling. Morphological features of mitochondria were assessed *via* transmission electron microscopy and immunofluorescence, and function was assessed by measuring oxidative capacity in primary hepatocytes, and respiratory control and proton leak in isolated mitochondria. Oxidative stress was measured by assessing activity and/or expression levels of *Nrf1*, *Sod1*, *Sod2*, catalase and 8-OHdG.

RESULTS

When challenged with AMLN diet for 12 wk, *ob/ob* and FATZO mice developed steatohepatitis in the presence of obesity and hyperinsulinemia. NASH development was associated with hepatic mitochondrial abnormalities, similar to those previously observed in humans, including mitochondrial accumulation and increased proton leak. AMLN diet also resulted in increased numbers of fragmented mitochondria in both strains of mice. Despite similar mitochondrial phenotypes, we found that *ob/ob* mice developed more advanced hepatic fibrosis. Activity of superoxide dismutase (SOD) was increased in *ob/ob* AMLN mice, whereas FATZO mice displayed increased catalase activity, irrespective of diet. Furthermore, 8-OHdG, a marker of oxidative DNA damage, was significantly increased in *ob/ob* AMLN mice compared to FATZO AMLN mice. Therefore, antioxidant capacity reflected as the ratio of catalase:SOD activity was similar between FATZO and C57BL6J control mice, but significantly perturbed in *ob/ob* mice.

CONCLUSION

Oxidative stress, and/or the capacity to compensate for increased oxidative stress, in the setting of mitochondrial dysfunction, is a key factor for development of hepatic injury and fibrosis in these mouse models.

Key words: Nonalcoholic steatohepatitis; Steatosis; Fibrosis; Mitochondrial function; Oxidative stress

Core tip: *ob*/*ob* and FATZO mice developed nonalcoholic fatty liver disease/nonalcoholic steatohepatitis (NASH) when fed a high *trans*-fat, high fructose and high cholesterol diet, in the context of obesity and insulin resistance, but showed differences in liver disease severity including collagen deposition and monocyte/macrophage infiltration. Mitochondrial dysfunction and increased numbers of mitochondria were observed in both models, similar to that reported in human NASH. Oxidative damage and antioxidant capacity were associated with disease severity. FATZO mice displayed increased catalase activity and reduced oxidative DNA damage compared to *ob*/*ob* mice, which may explain their lower disease burden.

Boland ML, Oldham S, Boland BB, Will S, Lapointe JM, Guionaud S, Rhodes CJ, Trevaskis JL. Nonalcoholic steatohepatitis severity is defined by a failure in compensatory antioxidant capacity in the setting of mitochondrial dysfunction. *World J Gastroenterol* 2018; 24(16): 1748-1765 Available from: URL: http://www.wjgnet.com/1007-9327/full/v24/i16/1748.htm DOI: http://dx.doi.org/10.3748/wjg.v24.i16.1748

INTRODUCTION

Non-alcoholic fatty liver disease (NAFLD), now the most common liver disease, encompasses a spectrum of disorders from benign simple fatty liver to the more severe non-alcoholic steatohepatitis (NASH) that can progress to liver cirrhosis and hepatocellular carcinoma. Given the strong association of NAFLD with obesity, type Ⅱ diabetes and other aspects of the metabolic syndrome, the current estimated NAFLD prevalence of 20%-40% worldwide is expected to increase[1-3]. While no FDA-approved pharmacotherapies for NAFLD/NASH currently exist, more than 100 clinical trials are now targeting this highly significant unmet medical need.

Insulin resistance is a major pathophysiological factor that underlies the strong association between obesity/type Ⅱ diabetes and NAFLD. Increased circulating free fatty acids and *de novo* lipogenesis lead to excess lipid storage in the hepatocyte, and accumulation of intrahepatic lipid is linked to pathogenic insulin resistance and subsequent onset of type 2 diabetes. This lipid overload also places a unique burden on the mitochondria and promotes mitochondrial dysfunction *in vitro* and in animal models. Data from multiple studies suggest that while TCA cycle activity is increased in NAFLD, mitochondrial respiratory chain inefficiencies lead to increased generation of reactive oxygen species (ROS) and lipotoxic intermediates that further promote oxidative damage and inflammation[4-7]. Importantly, while increased hepatic mitochondrial respiration was observed in obese patients with and without fatty liver, this increase was lost in obese patients with NASH and was associated with increased mitochondrial content, proton leakage and oxidative stress[8].

While dysregulated mitochondrial metabolism has been implicated in NALFD pathogenesis and progression, the specific contribution to disease etiology remains an active area of investigation[9,10]. Multiple lines of evidence suggest that therapeutically targeting the mechanisms leading to mitochondrial dysfunction may improve liver disease[10,11]. The use of pre-clinical models that mimic human pathology in the context of known risk factors, including obesity and insulin resistance, are necessary to understand the clinical translatability of pharmacological interventions given the difficulty of studying humans with a slow progressing disease that cannot be confirmed non-invasively[12].

Hepatic mitochondrial function and oxidative stress in metabolically-relevant, pre-clinical models of simple fatty liver *vs* NASH have not been fully assessed. Here,

two pre-clinical mouse models of simple steatosis and NASH were investigated: *ob/ob* mice on NASH-inducing AMLN diet[13], and the recently described polygenic FATZO mouse which develops high-fat diet-induced obesity and impaired glucose tolerance and which retains an intact leptin axis[14,15]. Importantly, these models are readily available and rapidly and consistently develop clinically relevant disease. We characterized the contribution of mitochondria and oxidative stress to disease phenotype and demonstrate that a reduced ability to combat oxidative stress in the setting of mitochondrial dysfunction is associated with the progression to NASH with advanced fibrosis. These data highlight the utility of these models to dissect the underlying pathobiology of NAFLD disease progression and to predict pharmacological efficacy.

MATERIALS AND METHODS

Animals

Animal studies were conducted in accordance with protocols approved by the Institutional Animal Care and Use Committee (IACUC) at MedImmune and in compliance with the applicable national laws and regulations concerning use of laboratory animals and the AstraZeneca Animal Welfare and Bioethics policies. Eight-week old male C57BL6J or *Lep*^{ob}/*Lep*^{ob} (*ob*/*ob*) mice (Jackson labs, Bar Harbor, ME, United States) and 8-week-old male FATZO mice (Crown Bioscience, Indianapolis, IN, United States) were housed in standard caging at 22 ℃ in a 12-h light: 12-h dark cycle at standard temperature and humidity conditions with *ad libitum* access to water and food. Mice were maintained on test diets for 12 wk. The following test diets were used: 2018 Tekland rodent diet (Envigo, United States), low-fat diet (LFD; 10% kcal/fat; D09100304, Research Diets, New Brunswick, NJ, United States) and the Amylin Liver NASH (AMLN) diet high in fat (40% kcal), fructose (22% by weight), and cholesterol (2% by weight) (D09100301 Research Diets). Study groups comprised C57BL6J chow fed (lean) mice (n = 6), *ob*/*ob* mice on LFD (n = 8) and *ob*/*ob* mice on AMLN diet (n = 10), or C57BL6J lean mice, FATZO mice on LFD, or FATZO mice on AMLN diet (all n = 5 per group).

Measurement of plasma ALT

Terminal blood was collected in EDTA-coated tubes and centrifuged at 10000 × g for 10 min. The plasma was collected and analyzed for ALT levels using a biochemistry analyzer (Cobas c-111, Roche Diagnostics, Indianapolis, IN, United States).

Liver lipid quantification

Total lipids were measured in liver samples using a Bruker LF-90 minispec system (Bruker Biospin Corporation, Billerica, MA, United States). The data are expressed as the percent lipid relative to the total tissue mass.

Plasma insulin and pancreatic insulin content

To isolate pancreatic insulin, the tissue was incubated in a 1.5% HCl/70% EtOH solution overnight at -20 ℃. The tissue was homogenized and frozen again overnight at -20 ℃. Following centrifugation at 2000 rpm for 15 min, the aqueous layer was transferred to a new tube and neutralized upon the addition of 1 mol/L Tris, pH 7.5 at a 1:1 ratio. Plasma and pancreatic insulin levels were measured *via* immunoassay (K152BZC, MesoScale Diagnostics, Rockville, MD, United States).

Histological analysis and quantification of liver tissue

Livers were fixed in 10% neutral buffered formalin for 24 h. Paraffin-embedded tissue sections were stained with hematoxylin and eosin using standard procedures. Histological assessments were conducted by a pathologist under blinded conditions. A modified scoring system, based on the Brunt and Kleiner NAFLD activity score, previously developed and validated to enable a more reproducible and semi-quantitative assessment of murine liver was used to quantify various parameters of liver phenotype[16]. The following parameters were graded to generate the overall NASH score: macrovesicular steatosis (0: < 5%, 1: 5%-33%, 2: 34%-66%, 3: > 66%); ballooning degeneration (0 = absent, 1 = present); lobular inflammation (0 = no foci, 1 = rare foci, 2 = occasional foci, 3 = frequent foci); biliary hyperplasia (0 = none, 1 = mild, 2 = prominent); CD68 immunoreactivity (0 = normal, 1 = minimal increased, 2 = more than minimal increase).

Customized algorithms (Definiens, Munich, Germany) were applied to the liver sections to quantify macrosteatosis per liver area, total collagen area and number of CD68-positive cells. White spaces, non-native liver tissues, large blood vessels and bile ducts were excluded from the analyses.

Immunohistochemistry

Immunohistochemistry was performed using a Ventana Discovery ULTRA Staining Module (Ventana Medical Systems, Tucson, AZ, United States). Formalin-fixed, paraffin embedded liver sections were stained with anti-CD68 (ab125212 Abcam, Cambridge, MA, United States), anti-collagen type 1 A1 (1310-01 Southern Biotech, Birmingham, AL, United States), or anti-catalase (PA5-29183, ThermoFisher).

Transmission electron microscopy

Freshly isolated liver was chemically fixed in 0.1 mol/L cacodylate buffer containing 4% paraformaldehyde and 2% glutaraldehyde. Samples were resin-embedded, sectioned, and stained as previously described[17]. Samples were imaged using the FEI Tecnai G2 SPIRIT electron microscope equipped with a CCD camera (Pleasanton, CA, United States) at 120000 V. Images were acquired using GATAN digital micrograph software (Warrendale, PA, United States). Electron micrographs

were viewed in a blinded fashion using 3Dmod software[18] on a Wacom Cintiq 22HD art tablet (Vancouver, WA, United States). Mitochondrial area and number were quantified per total cytoplasmic area from ⩾ 10 electron micrographs per group *via* manual tracing using the art tablet as previously described (N ⩾ 3 biological replicates, ⩾ 1.5 mm^2 total cytoplasmic area)[19].

Immunofluorescence

FFPE liver sections were deparaffinized followed by blocking of endogenous peroxidases. Antigen retrieval was carried out by heating samples at 119 C for 6.5 min in citrate buffer solution (Dako Target Retrieval Solution, Agilent Technologies, Santa Clara, CA, United States). After blocking with 1.5% horse serum, slides were incubated overnight in anti-HSP60 (D6F1, Cell Signaling Technology, Danvers, MA, United States) in Dako antibody diluent (S3022, Agilent Technologies). Secondary antibody incubation with goat anti-rabbit Alexa 488 (ThermoFisher) was carried out at room temperature for 1 h. Slides were mounted using Prolong Gold plus DAPI (ThermoFisher). Slides were imaged using a Leica TCS SP5 X confocal microscope. Confocal images were viewed in a blinded fashion using 3Dmod software on a Wacom Cintiq 22HD art tablet (Vancouver, WA, United States). Mitochondrial length and number per total cytoplasmic area were quantified from ⩾ 15 images per group (n ⩾ 3 biological replicates) *via* manual tracing of cell boundaries, nuclei, lipid droplets and mitochondria. Total cytoplasmic area was calculated as area within the cell boundary minus the nuclei and lipid droplet areas.

Primary hepatocyte isolation

Murine primary hepatocytes were isolated using a modified two-step non-recirculating perfusion method as previously described[20]. All assays were carried out within 18-24 h post-plating.

Mitochondrial oxygen consumption

Mitochondrial oxygen consumption was measured using the Seahorse Xfe96 analyzer (Agilent Technologies). Primary hepatocytes were plated at a density of 7500 cells per well and allowed to recover overnight. The medium was exchanged (DMEM containing 5 mmol/L glucose, 4 mmol/L L-glutamine, 2 mmol/L sodium pyruvate, pH 7.4) and the plate was placed in a CO_2-free incubator for 30 min prior to being placed in the analyzer. The following compounds were used in the mitochondrial stress test: 1 μmol/L oligomycin (Sigma, St Louis, MO, United States), 0.5 μmol/L FCCP (Sigma), and 5 μmol/L antimycin A (Sigma). The data represent the average of three independent experiments each with a minimum of 8 replicates per group.

Mitochondrial coupling and proton leak

The respiratory control ratio (RCR) and leak control ratio (LCR) were quantified using freshly isolated hepatic mitochondria as an index of mitochondrial coupling and proton leak, respectively[8]. Briefly, 5 μg of mitochondria were loaded per well of the seahorse plate in assay medium (70 mmol/L sucrose, 220 mmol/L mannitol, 10 mmol/L KH_2PO_4, 5 mmol/L $MgCl_2$, 2 mmol/L HEPES, 1 mmol/L EGTA, 0.2% (w/v) fatty acid-free BSA, pH 7.2 supplemented with complex Ⅱ substrate succinate at 10 mmol/L). The following injections were performed: 4 mmol/L ADP (state 3), 1 μmol/L oligomycin (state 3_o), 1 μmol/L FCCP (state 3_U) and 4 μmol/L antimycin A/ 2 μmol/L rotenone. RCR is represented by the ratio of ADP-stimulated respiration (state 3) to respiration in the presence of oligomycin (state 3_o), and LCR is represented by the ratio of respiration in the presence of oligomycin (State 3_o) to FCCP-stimulated respiration (state 3_U).

Citrate synthase activity

Mitochondrial content was quantified by citrate synthase activity (CSA) of freshly isolated primary hepatocytes or liver mitochondria using the Citrate Synthase Activity Colorimetric Assay Kit (BioVision, Milpitas, CA, United States) according to the manufacturer's instructions and normalized to total protein assessed by the Pierce BCA protein assay kit (ThermoFisher).

Isolation of liver mitochondria

Excised liver was rinsed in several changes of PBS and homogenized in ice cold isolation buffer (70 mmol/L sucrose, 210 mmol/L mannitol, 5 mmol/L HEPES, 1 mmol/L EGTA, 0.5% w/v fatty acid-free BSA, pH 7.2) using a Wheaton™ Dounce Tissue Grinder (Fisher Scientific). After centrifugation at 800 x g for 10 min at 4 ℃, the supernatants were collected and centrifuged at 8000 × g for 10 min at 4 ℃. The resulting mitochondrial pellet was washed two times and resuspended in a minimal volume of isolation buffer. The isolated mitochondria were kept on ice until use. Protein concentration was determined using the Pierce BCA Protein Assay Kit (ThermoFisher).

RNA isolation and real-Time PCR

Total liver RNA and genomic DNA were isolated using standard procedures. Qiagen RNeasy® columns (Qiagen, United States) were used for RNA purification according to the manufacturer's protocol, including an on-column DNA digestion using DNaseI. Equal amounts of RNA were reverse transcribed to cDNA using SuperScript Ⅲ First Strand cDNA synthesis kit (Invitrogen, Carlsbad, CA, United States) according to the manufacturer's instructions. Real-Time PCR was performed on a QuantStudio-7 Flex System (Applied Biosystems, Foster City, CA, United States) using Applied Biosystems TaqMan Fast Universal PCR Master Mix and TaqMan probes. Each sample was assayed in triplicate and quantified using the ΔΔCT method normalized to endogenous control *Ppia* (mRNA) or nuclear encoded gene β-globin (gDNA). The following Taqman probes were used in qPCR assays: collagen type 1 alpha 1 (Col1a1, Mm00801666_g1), collagen type 1 alpha 2

(Col1a2, Mm00483888_m1), TIMP metallopeptidase inhibitor 1 (Timp1, Mm01341361_m1), interleukin 1 beta (Il1b, Mm00434228_m1), cluster of differentiation 68 (Cd68, Mm03047343_m1), tumor necrosis factor alpha (Tnf, Mm00443258_m1), PPARG coactivator 1 alpha (Ppargc1a, Mm01208835_m1), nuclear respiratory factor 1 (Nrf1, Mm01135606_m1), transcription factor A, mitochondrial (Tfam, Mm00447485_m1), superoxide dismutase 1, soluble (Sod1, Mm1344233_g1), superoxide dismutase 2, mitochondrial (Sod2, Mm01313000_m1), catalase (Cat, Mm00437992_m1), glutathione peroxidase (Gpx1, Mm00656767_g1), and peptidylprolyl isomerase A (Ppia, Mm02342430_g1).

Oxidative stress assays

Superoxide dismutase activity (7501-500-K, Trevigen, Gaithersburg, MD, United States) and catalase activity (707002, Cayman Chemical, Ann Arbor, MI, United States) were measured in freshly prepared liver homogenates according to the manufacturer's protocols. The levels of 8-hydroxydeoxyguanosine (8-OHdG) were measured *via* ELISA using approximately 20 μg of total hepatic genomic DNA (4380-096-K, Trevigen).

Statistical analysis

All statistical analyses were carried out using GraphPad Prism 7 (GraphPad Software, San Diego, CA, United States). The data were analyzed *via* one-way or two-way ANOVA and Tukey's post-test. Data are shown as the mean ± SE. Values of $P \leq 0.05$ were considered significant.

RESULTS

Ob/ob mice develop NASH with fibrosis in the setting of obesity and insulin resistance

NASH induction was assessed in *ob/ob* mice, a proposed NASH model when challenged with AMLN diet. C57BL6J mice served as healthy age-matched controls (lean) and were compared to *ob/ob* mice maintained on LFD (*ob/ob* LFD) or AMLN diet (*ob/ob* AMLN) for 12 wk. After the 12-wk disease induction period, *ob/ob* LFD and *ob/ob* AMLN mice weighed significantly more than lean controls ($P < 0.0001$), but did not significantly differ from one another (Figure 1A). While non-fasting blood glucose was slightly reduced in *ob/ob* AMLN animals compared to lean controls (132 mg/dL *vs* 186 mg/dL, $P < 0.05$; Figure 1B), plasma insulin levels ($P < 0.05$; Figure 1C) and pancreatic insulin content ($P < 0.01$; Figure 1D) were concomitantly increased.

We measured markers associated with NAFLD including liver weight, liver lipid, and plasma alanine aminotransferase (ALT). Liver weight was significantly greater in *ob/ob* LFD *vs* lean animals (8.6% *vs* 4.5%, $P < 0.0001$), and was further increased in *ob/ob* AMLN animals (12.7%, $P < 0.0001$; Figure 2A). Similarly, *ob/ob* AMLN livers contained approxiately 34% intrahepatic lipid, which was significantly greater than livers from *ob/ob* LFD (25% lipid, $P < 0.0001$) and lean animals (5% lipid, $P < 0.0001$; Figure 2B). Plasma ALT was also significantly increased in *ob/ob* LFD *vs* lean animals (771 U/L *vs* 160 U/L, $P < 0.0001$) and was further elevated in *ob/ob* AMLN animals (1160 U/L, $P < 0.001$ *vs ob/ob* LFD; Figure 2C).

Macrovesicular steatosis was prominent in both *ob/ob* LFD (60%) and *ob/ob* AMLN animals (67%, $P < 0.001$ *vs ob/ob* LFD; Figure 2D). Hepatic fibrosis assessed by quantification of type 1 collagen stained area was significantly greater in *ob/ob* LFD *vs* lean livers ($P < 0.01$) and even greater in *ob/ob* AMLN liver ($P < 0.0001$ *vs ob/ob* LFD) (Figure 2E). Immunolabeling with the monocyte/macrophage marker CD68 was also markedly elevated in *ob/ob* AMLN livers compared to *ob/ob* LFD and lean controls ($P < 0.0001$ *vs ob/ob* LFD; Figure 2F).

We analyzed hepatic transcript levels of genes involved in fibrosis and inflammation that differentiate the more benign disease observed in *ob/ob* LFD liver histopathology from the steatohepatitis observed in *ob/ob* AMLN livers. Transcripts encoding the most abundant form of liver collagen, type 1 (*Col1a1* and *Col1a2*), in addition to type 3 collagen (*Col3a1*) were significantly elevated in *ob/ob* AMLN livers *vs* lean and *ob/ob* LFD livers ($P < 0.001$, $P < 0.01$, $P < 0.0001$, respectively, *vs ob/ob* LFD; Figure 2G). *Timp1*, another gene associated with increased extracellular matrix turnover, was significantly elevated in *ob/ob* AMLN compared to *ob/ob* LFD and lean livers ($P < 0.001$ *vs ob/ob* LFD; Figure 2G). The expression of cytokines including *Tgfb*, *Tnf*, *Il1b*, and *Il10*, and chemokines including *Ccl2*, *Ccl3*, and *Ccl11* were similarly upregulated in *ob/ob* AMLN livers compared to *ob/ob* LFD and lean controls ($P < 0.01$, $P < 0.05$, $P < 0.05$, $P = 0.2$; $P < 0.01$, $P < 0.001$, $P < 0.01$, respectively, *vs ob/ob* LFD; Figure 2H). Additionally, *Lgals3*, a marker associated with multiple inflammatory cell types and thought to contribute to fibrogenesis, was highly expressed in the livers of *ob/ob* AMLN but not lean or *ob/ob* LFD mice (30-fold induction *vs* lean controls, $P < 0.001$ *vs ob/ob* LFD; Figure 2H).

The steatosis grade was significantly higher in *ob/ob* LFD (grade 2.5, $P < 0.0001$) and *ob/ob* AMLN (grade 3, $P < 0.0001$) compared to lean livers (grade 0; Figure 3A). A significant increase in the number of inflammatory foci (Figure 3B), biliary hyperplasia (Figure 3C) and CD68-positive cells (Figure 3D) was observed in *ob/ob* AMLN *vs* lean ($P < 0.0001$) and *ob/ob* LFD livers ($P < 0.0001$). Ballooned hepatocytes were only observed in *ob/ob* AMLN livers (Figure 3E). An integrated NASH score was generated by combining the grades of steatosis, inflammation, biliary hyperplasia, CD68 positive cells, and ballooning degeneration (Figure 3F), which reflected the clear distinction between *ob/ob* LFD and *ob/ob* AMLN liver histopathology.

Fragmented mitochondria in ob/ob AMLN hepatocytes

We examined mitochondrial ultrastructure in livers from lean, *ob/ob* LFD and *ob/ob* AMLN mice by transmission

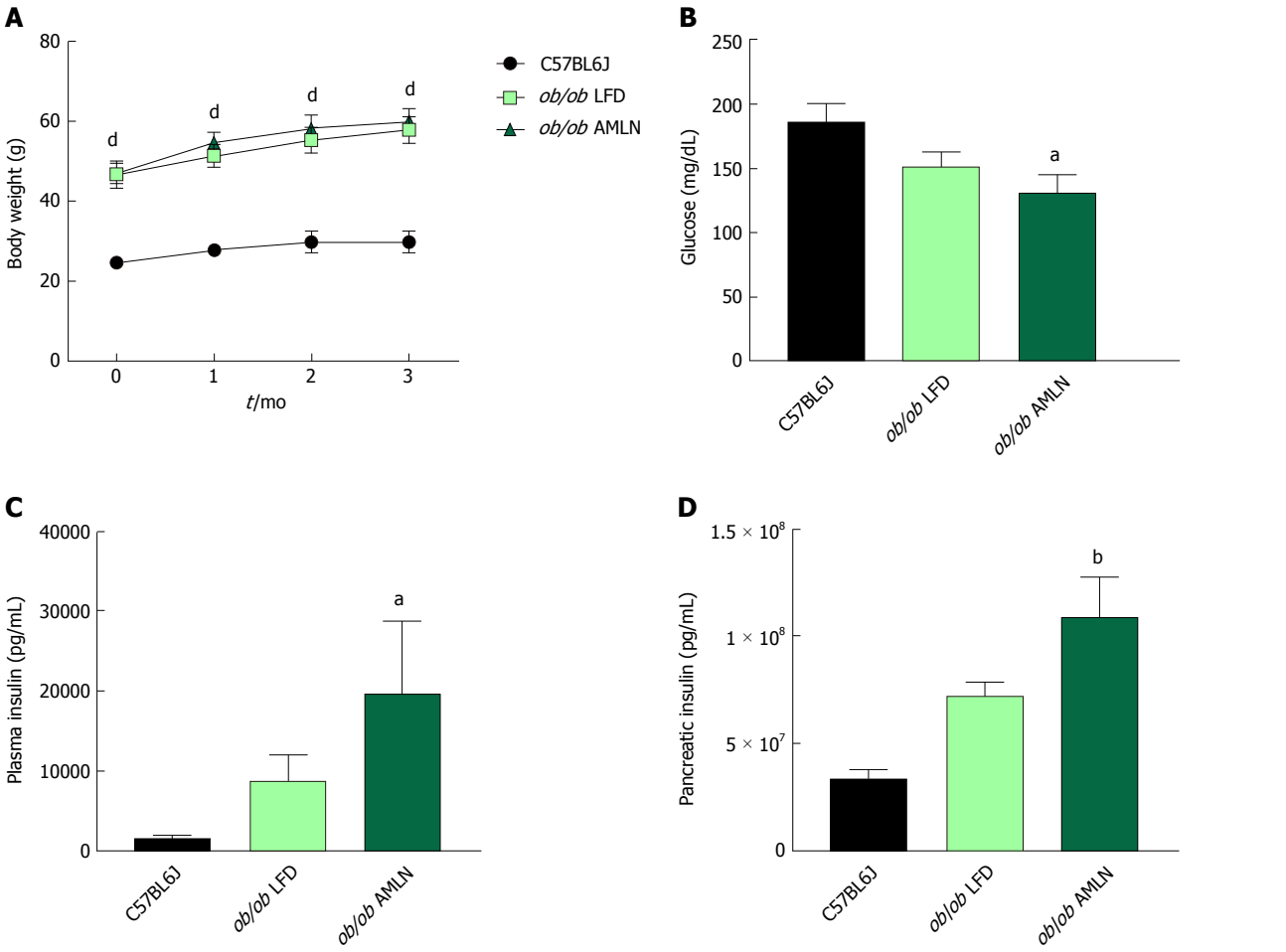

Figure 1 Obese *ob/ob* mice display increased hyperinsulinemia on AMLN diet. (A): Average body weight over 12-wk disease induction period; (B): Terminal non-fasting blood glucose levels; (C): Terminal non-fasting plasma insulin levels; (D): Pancreatic insulin content. $^{a}P \leq 0.05$, $^{b}P \leq 0.01$, $^{d}P \leq 0.0001$ *vs* C57BL6J. LFD: Low-fat diet.

electron micrography (TEM; Figure 4A). Quantitative assessment of TEM images showed *ob/ob* AMLN hepatocytes had increased numbers of mitochondria (approximately 1.5-fold, $P < 0.001$ *vs ob/ob* LFD; Figure 4B). While lean and *ob/ob* LFD hepatocytes contained a mixture of elongated and fragmented mitochondria, *ob/ob* AMLN hepatocytes contained smaller, more fragmented mitochondria (average area = 70 μm^2 for lean controls *vs* 45 μm^2 for *ob/ob* AMLN, $P < 0.01$; Figure 4C); however, no overt defects in outer membrane integrity or cristae formation were observed. Similarly, quantification of mitochondrial length and number from HSP60 immunostained liver sections revealed increased numbers of mitochondria overall in *ob/ob* AMLN livers ($P < 0.005$ *vs* lean controls; Figure 4D) and a significant increase in shorter, more fragmented mitochondria (Figure 4E). Citrate synthase activity (CSA), another measure of mitochondrial content, was increased over 2-fold in primary hepatocytes isolated from *ob/ob* AMLN mice *vs* lean controls ($P < 0.05$; Figure 4F). In line with smaller mitochondria in *ob/ob* AMLN hepatocytes, the expression of proteins required for mitochondrial fusion, mitofusin 1 (*Mfn1*) and dynamin-like 120 kDa protein, mitochondrial (*Opa1*), was significantly decreased in *ob/ob* AMLN livers compared to lean controls ($P < 0.01$ and $P < 0.05$, respectively; Supplementary Figure 4G).

To assess whether this increase in mitochondrial number was due to increased biogenesis, we quantified the expression of transcription factors required for mitochondrial biogenesis and components of the electron transport chain (ETC). While the expression of PPARγ-coactivator 1a (*Ppargc1a*) was slightly increased in *ob/ob* LFD livers (1.4-fold, $P = 0.06$ *vs* lean controls), it was unchanged in *ob/ob* AMLN *vs* lean livers (data not shown). Similarly, nuclear respiratory factor 1 (*Nrf1*) and mitochondrial transcription factor A (*Tfam*) mRNA levels were unchanged in *ob/ob* AMLN *vs* lean and *ob/ob* LFD livers (data not shown). Additionally, expression of mitochondrial autophagy genes *Bnip3*, *Park2* and *Pink1* was not different between groups (Figure 4G). Although *ob/ob* AMLN hepatocytes displayed increased mitochondrial number, they contained significantly less mitochondrial DNA (mtDNA) as assessed by the expression of mitochondrially-encoded genes *Cytb* and *Nd-1* relative to the expression of nuclear encoded β-globin (approximately 30% reduction, $P < 0.05$ *vs* lean controls; Supplementary Figure 4H).

Hepatic ob/ob AMLN mitochondria have reduced respiratory capacity and increased proton leak

To assess mitochondrial function, oxygen consumption of intact primary hepatocytes from lean, *ob/ob* LFD

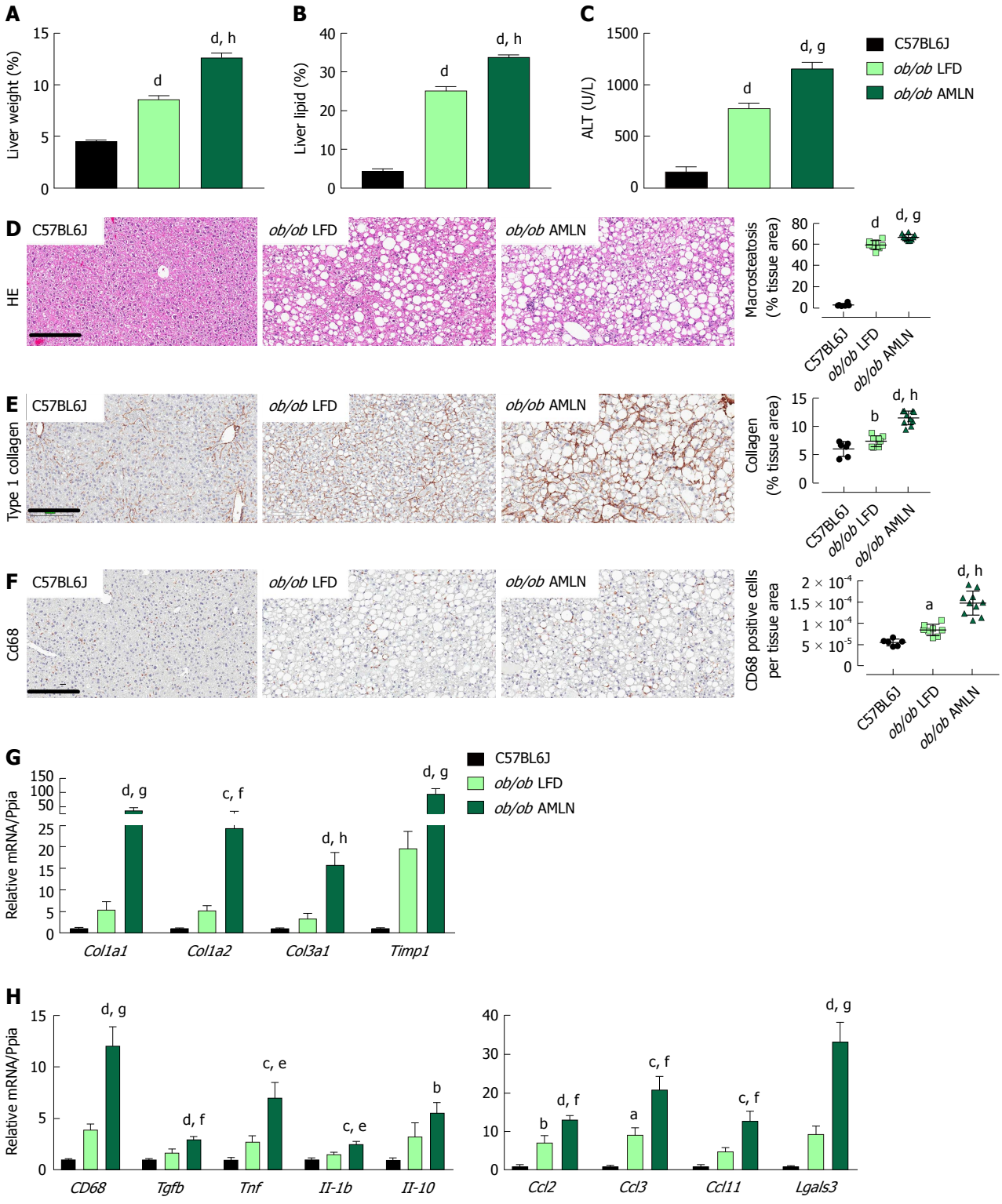

Figure 2 Comparison of metabolic and hepatic abnormalities associated with diet-induced nonalcoholic fatty liver disease/nonalcoholic steatohepatitis in *ob/ob* mice. Liver weight (A), liver lipid (B), and plasma alanine aminotransferase (ALT) levels (C) of lean (C57BL6J) and *ob/ob* mice maintained on control low-fat diet (*ob/ob* LFD) or AMLN diet (*ob/ob* AMLN) for 12 wk; (D): Representative hematoxylin and eosin stained liver sections and quantification of percentage of liver area containing macrosteatosis; (E): Representative collagen type 1 alpha 1 stained liver sections and quantification of collagen area. Scale bar = 200 μm; (F): Representative CD68-stained liver sections and quantification of CD68-positive cells; G, H: Relative expression of genes associated with fibrosis and inflammation. $^{a}P \leq 0.05$, $^{b}P \leq 0.01$, $^{c}P \leq 0.001$, $^{d}P \leq 0.0001$ *vs* C57BL6J; $^{e}P \leq 0.05$, $^{f}P \leq 0.01$, $^{g}P \leq 0.001$, $^{h}P \leq 0.0001$ *vs* LFD. LFD: Low-fat diet.

and *ob/ob* AMLN animals was measured (Figure 5A). *ob/ob* AMLN hepatocytes displayed significantly reduced basal respiration that was approximately 50% lower compared to lean ($P < 0.01$) and *ob/ob* LFD hepatocytes ($P < 0.05$) (Figure 5B). Maximal mitochondrial respiratory capacity was significantly

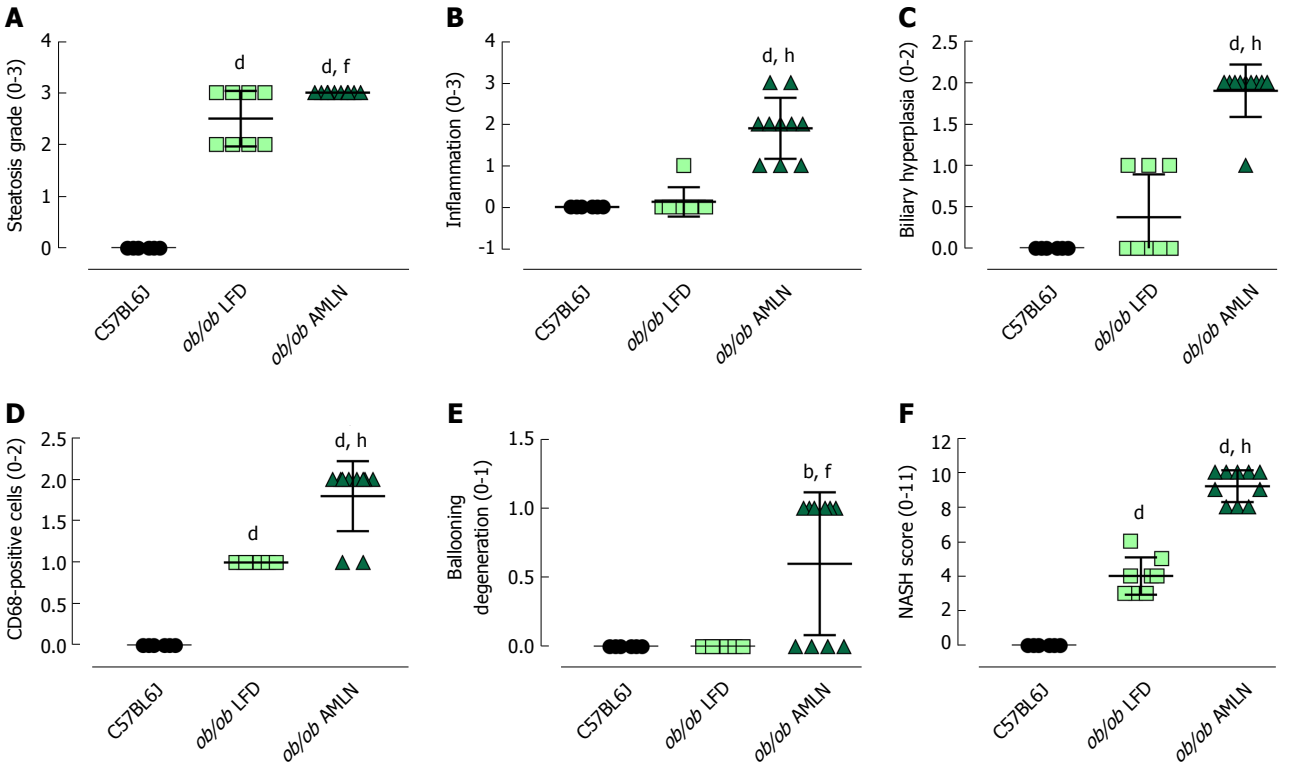

Figure 3 Histopathological grading of C57BL6J, *ob/ob* low-fat diet and *ob/ob* AMLN liver. Individual grades of steatosis (A), inflammation (B), biliary hyperplasia (C), CD68-positive cells (D) and ballooning degeneration (E) are shown; (F): Comparison of the total NASH scores representing the sum of all histologic parameters. $^{b}P \leqslant 0.01$, $^{d}P \leqslant 0.0001$ *vs* C57BL6J; $^{f}P \leqslant 0.01$, $^{h}P \leqslant 0.0001$ *vs* LFD. LFD: Low-fat diet.

increased in *ob/ob* LFD compared to lean hepatocytes (+45%, $P < 0.05$; Figure 5B). In contrast, *ob/ob* AMLN hepatocytes displayed significantly reduced maximal respiration compared to lean (-45%, $P < 0.05$) and *ob/ob* LFD hepatocytes (-60%, $P < 0.001$; Figure 5B).

We also assessed mitochondrial coupling and proton leak. The mitochondrial respiratory control ratio (RCR) and leak control ratio (LCR) were quantified using isolated mitochondria from lean, *ob/ob* LFD and *ob/ob* AMLN livers. Mitochondria from *ob/ob* mouse liver displayed slightly increased proton leak without a significant decrease in respiratory control[21], and AMLN diet further increased proton leak and reduced RCR. Mitochondrial coupling was decreased in *ob/ob* AMLN mice compared to mitochondria from lean mice (4.2 *vs* 5.6; Figure 5C), although this difference did not reach statistical significance. *ob/ob* AMLN mitochondria also displayed a higher LCR compared to lean controls (0.35 *vs* 0.23, $P = 0.06$; Figure 5D), indicating increased proton leak.

FATZO mice fed AMLN diet display enhanced microvesicular steatosis and lobular inflammation but minimal fibrosis

While the *ob/ob* mouse exhibits key aspects of human metabolic disease and, importantly, develops diet-induced NASH with consistent grade 2-3 fibrosis, most humans with NAFLD/NASH are likely hyperleptinemic as opposed to leptin-deficient. We therefore investigated the FATZO mouse, an inbred polygenic cross of AKR/J and C57BL6J strains with a predisposition to obesity and insulin resistance, but intact leptin axis[14,15].

After 12 wk on diet, FATZO mice fed LFD (FATZO LFD) weighed significantly more than lean (C57BL6J) controls (43 g *vs* 35 g, $P < 0.0001$), while FATZO mice fed AMLN diet (FATZO AMLN) weighed significantly more than both FATZO LFD and lean controls (50 g, $P < 0.001$ *vs* FATZO LFD; Figure 6A). Plasma glucose was slightly elevated in FATZO LFD (271 mg/dL) and FATZO AMLN mice (236 mg/dL) compared to lean controls (186 mg/dL; Figure 6B). FATZO AMLN mice displayed severe hyperinsulinemia with average plasma insulin levels that were significantly greater compared to FATZO LFD and lean controls ($P < 0.01$ for *ob/ob* AMLN *vs* lean controls; Figure 6C). Both FATZO LFD and FATZO AMLN mice had increased pancreatic insulin content, which was significantly greater in FATZO AMLN mice compared to lean controls (+50%, $P < 0.05$; Figure 6D).

Markers of liver disease including hepatomegaly, hepatic steatosis and elevated plasma ALT levels were present in both FATZO LFD and FATZO AMLN mice. Relative liver weight was significantly increased in FATZO LFD *vs* lean animals (7.3% *vs* 4.4%, $P < 0.0001$), and was further increased in FATZO AMLN animals (10.6%, $P < 0.001$ *vs* FATZO LFD) (Figure 7A). Similarly, hepatic lipid content was significantly greater in FATZO LFD compared to lean controls (20% *vs* 6%) and was greatest in FATZO AMLN mice (30%, $P < 0.0001$ *vs* FATZO LFD; Figure 7B). Plasma ALT was also significantly increased in FATZO LFD *vs* lean animals

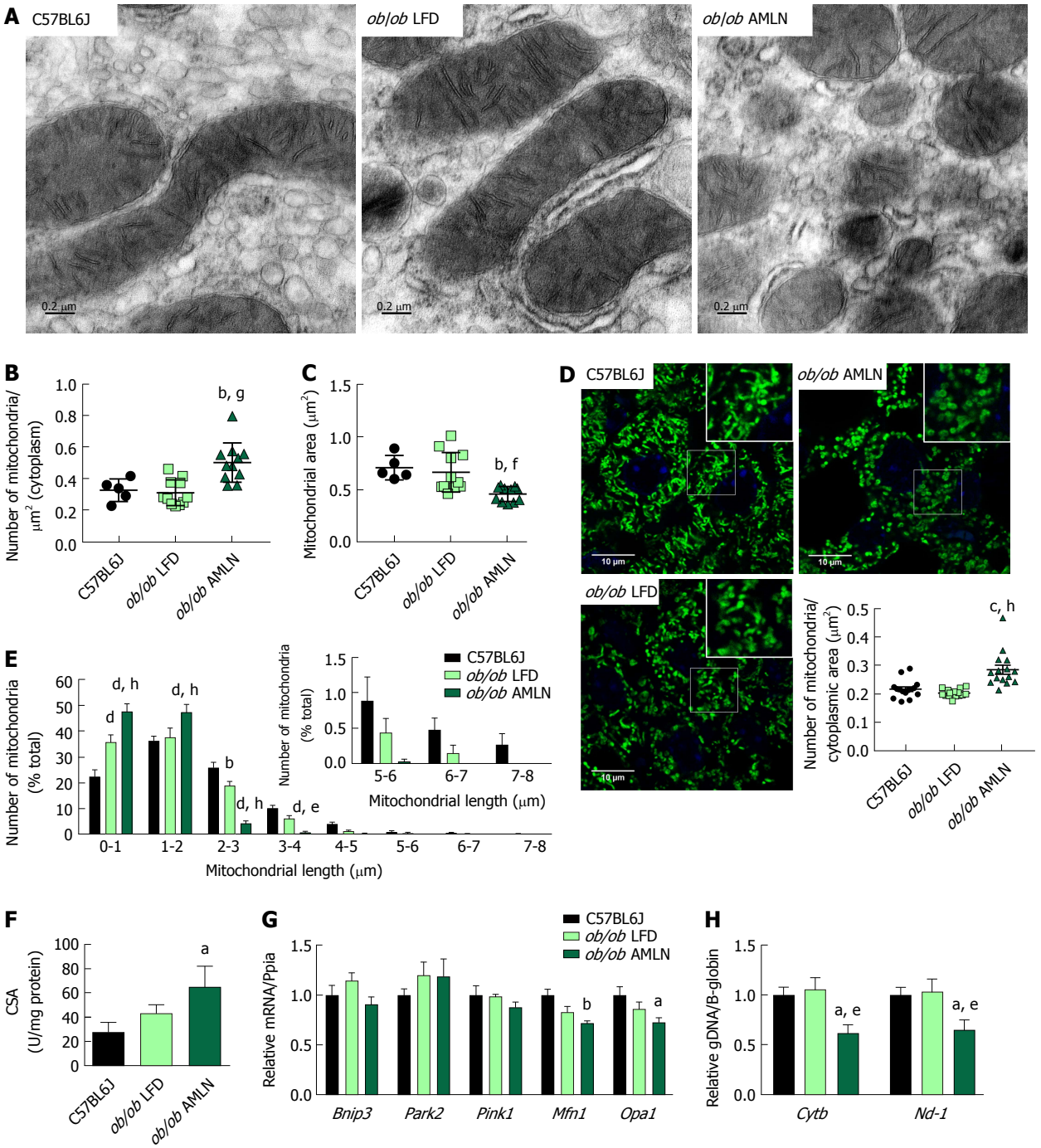

Figure 4 ***ob/ob*** **AMLN hepatocytes display increased numbers of fragmented mitochondria.** (A) Transmission electron micrographs (TEM) showing mitochondrial morphology and ultrastructure in the liver. Scale bar = 0.2 μm. Quantification of the number of mitochondria (B) and mitochondrial area (C) from TEM images; (D): Confocal images of HSP60 stained liver sections and quantification of mitochondrial number per cytoplasmic area. Scale bar = 10 μm; (E): Histogram depicting the number of mitochondria per binned mitochondrial length as a percentage of total mitochondria per cell; (F): Mitochondrial content measured by citrate synthase activity in isolated primary hepatocytes; (G): Relative hepatic expression of genes associated with mitophagy; (H): Quantification of mitochondrial genome-encoded *CytB* or *Nd1* relative to nuclear-encoded β-globin from total genomic DNA extracted from the liver. $^{a}P \leq 0.05$, $^{b}P \leq 0.01$, *vs* C57BL6J; $^{e}P \leq 0.05$, $^{f}P \leq 0.01$, $^{g}P \leq 0.001$, $^{h}P \leq 0.0001$ *vs* LFD. LFD: Low-fat diet.

(260 U/L *vs* 50 U/L, $P < 0.0001$) and was further elevated in FATZO AMLN animals (370 U/L, $P < 0.01$ *vs* FATZO LFD; Figure 7C), but was nonetheless still much lower than levels observed in *ob/ob* AMLN mice (>1100 U/L, Figure 1C).

Assessment of HE-stained liver samples revealed the presence of prominent steatosis, both micro- and macrovesicular, in both FATZO LFD and FATZO AMLN animals (Figure 7D). Increased macrophage/monocyte infiltration was also observed in FATZO LFD and FATZO AMLN mice (Figure 7E), paralleled by increased expression of hepatic *Cd68* (3.5-fold in FATZO LFD and 5.2-fold in FATZO AMLN; $P < 0.05$ FATZO LFD *vs* FATZO AMLN; Figure 7H). Mild collagen deposition was also

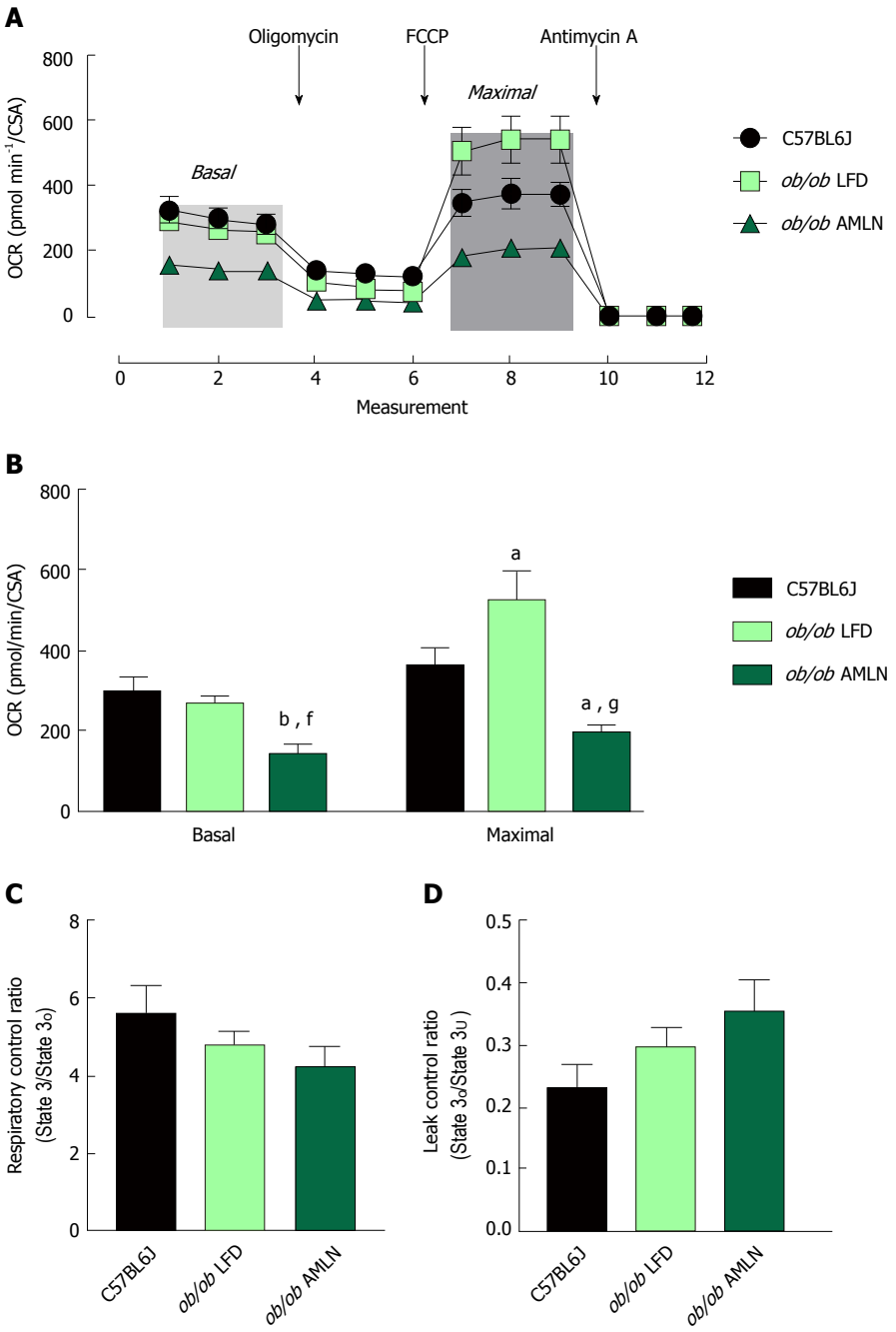

Figure 5 Mitochondria from *ob/ob* AMLN livers display reduced respiratory capacity and increased proton leak. (A): Oxygen consumption of primary hepatocytes isolated from C57BL6J, *ob/ob* LFD and *ob/ob* AMLN livers normalized to mitochondrial content (citrate synthase activity, CSA). Changes in mitochondrial respiration in response to oligomycin, FCCP and antimycin A are shown. Light grey box = basal respiration, dark grey box = maximal uncoupled respiration; (B): Quantification of baseline oxygen consumption (basal respiration) and FCCP-stimulated oxygen consumption (maximal respiration) normalized to CSA; (C): Mitochondrial respiratory control ratio, a measure of mitochondrial coupling, defined as state 3/ state o respiration of mitochondria isolated from the livers of C57BL6J, *ob/ob* LFD and *ob/ob* AMLN mice; (D): Mitochondrial leaking control ratio, a measure of proton leak, defined as state o/ state 3_U respiration. $^{a}P \leqslant 0.05$, $^{b}P \leqslant 0.01$, *vs* C57BL6J; $^{f}P \leqslant 0.01$, $^{g}P \leqslant 0.001$, *vs* LFD. LFD: Low-fat diet.

apparent in FATZO animals but did not worsen upon AMLN diet feeding (Figure 7F).

Transcriptional profiling of genes involved in hepatic fibrosis and inflammation revealed additional evidence of active liver disease in FATZO mice. Collagens including *Col1a1*, *Col1a2* and *Col3a1* were increased in FATZO LFD livers compared to lean controls (approximately 6-8-fold for each), and were further induced in FATZO AMLN livers (Figure 7G). All cytokines assayed including *Tgfb*, *Tnf*, *Il1b*, and *Il10*, and chemokines including *Ccl2*, *Ccl3*, and *Ccl11* were similarly upregulated in FATZO LFD livers compared to lean controls and even further induced in FATZO AMLN livers (Figure 7H). Additional fibrosis related genes *Timp1* and *Lgals3* were significantly elevated in FATZO LFD livers compared to lean controls, with even further induction observed in FATZO AMLN livers (Figure 7G, H). Integrated NASH scores generated from combining

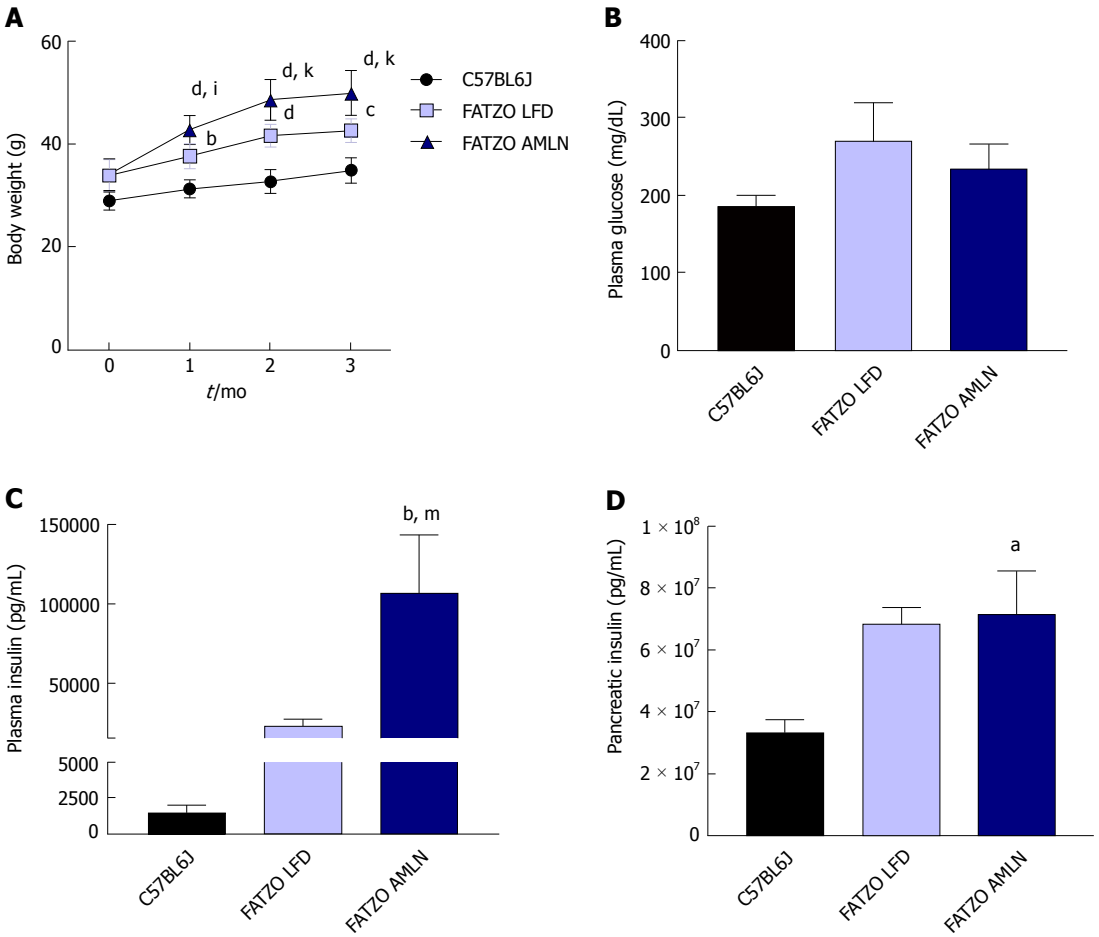

Figure 6 AMLN diet exacerbates obesity and hyperinsulinemia in FATZO mice. (A): Average body weight over 12-wk disease induction period; (B): Terminal non-fasting blood glucose levels; (C): Terminal non-fasting plasma insulin levels; (D): Pancreatic insulin content. $^{a}P \leq 0.05$, $^{b}P \leq 0.01$, $^{c}P \leq 0.001$, $^{d}P \leq 0.0001$ *vs* C57BL6J; $^{i}P \leq 0.05$, $^{k}P \leq 0.001$, FATZO LFD; $^{m}P \leq 0.05$, FATZO AMLN unless noted otherwise. LFD: Low-fat diet.

grades of steatosis (Figure 8A), inflammation (Figure 8B), biliary hyperplasia (Figure 8C), CD68-positive cells (Figure 8D) and hepatocyte ballooning (Figure 8E) were significantly greater for FATZO LFD and FATZO AMLN mice compared to lean controls, but did not significantly differ from one another (Figure 8F).

Increased mitochondrial fragmentation in FATZO mice is associated with mild mitochondrial dysfunction

Similar to *ob/ob* mice, FATZO AMLN mice displayed significantly increased numbers of fragmented mitochondria (Figure 9A, B) and hepatic CSA (Figure 9C) compared to FATZO LFD and lean controls. In contrast, this increase was associated with a significant induction of mitochondrial biogenesis genes in FATZO mice. *Nrf1* was consistently induced in both FATZO LFD and FATZO AMLN livers compared to lean controls ($P <$ 0.01 for FATZO LFD, $P < 0.0001$ for FATZO AMLN *vs* lean), *Ppargc1a* was significantly induced in FATZO LFD livers compared to lean controls (1.75-fold, $P < 0.001$) and *Tfam* was significantly induced in FATZO AMLN livers *vs* lean controls 1.4-fold, $P < 0.01$; Figure 9D). Additionally, decreased mitophagy may contribute to increased mitochondrial content, although only *Bnip3* expression was significantly reduced in FATZO LFD and FATZO AMLN livers compared to lean controls (-40%, $P < 0.05$ for FATZO LFD, -25%, $P = 0.08$ for FATZO AMLN *vs* lean) with no changes observed in *Park2* or *Pink1* expression (Supplementary Figure 9E). No differences in the mitochondrial:nuclear DNA ratio were observed (Figure 9F), suggesting that mtDNA replication is occurring normally in contrast to that observed in the *ob/ob* AMLN model.

To assess hepatic mitochondrial function in the FATZO mice we measured mitochondrial coupling and proton leak in isolated mitochondria. While there was a trend for reduced RCR in FATZO AMLN mitochondria compared to lean controls, this reduction was small and did not reach statistical significance (4.1 *vs* 4.9, $P = 0.5$; Figure 9G). Similar to the *ob/ob* models, both FATZO LFD and FATZO AMLN mitochondria displayed a trend for increased proton leak compared to lean controls (0.43 for both FATZO LFD and AMLN *vs* 0.32 for lean controls; $P = 0.08$ and $P = 0.07$, respectively; Figure 9H).

Ob/ob mice display a reduced ability to manage oxidative stress compared to FATZO mice

The oxidative stress responsive transcription factor *Nrf2* was significantly induced in both *ob/ob* and

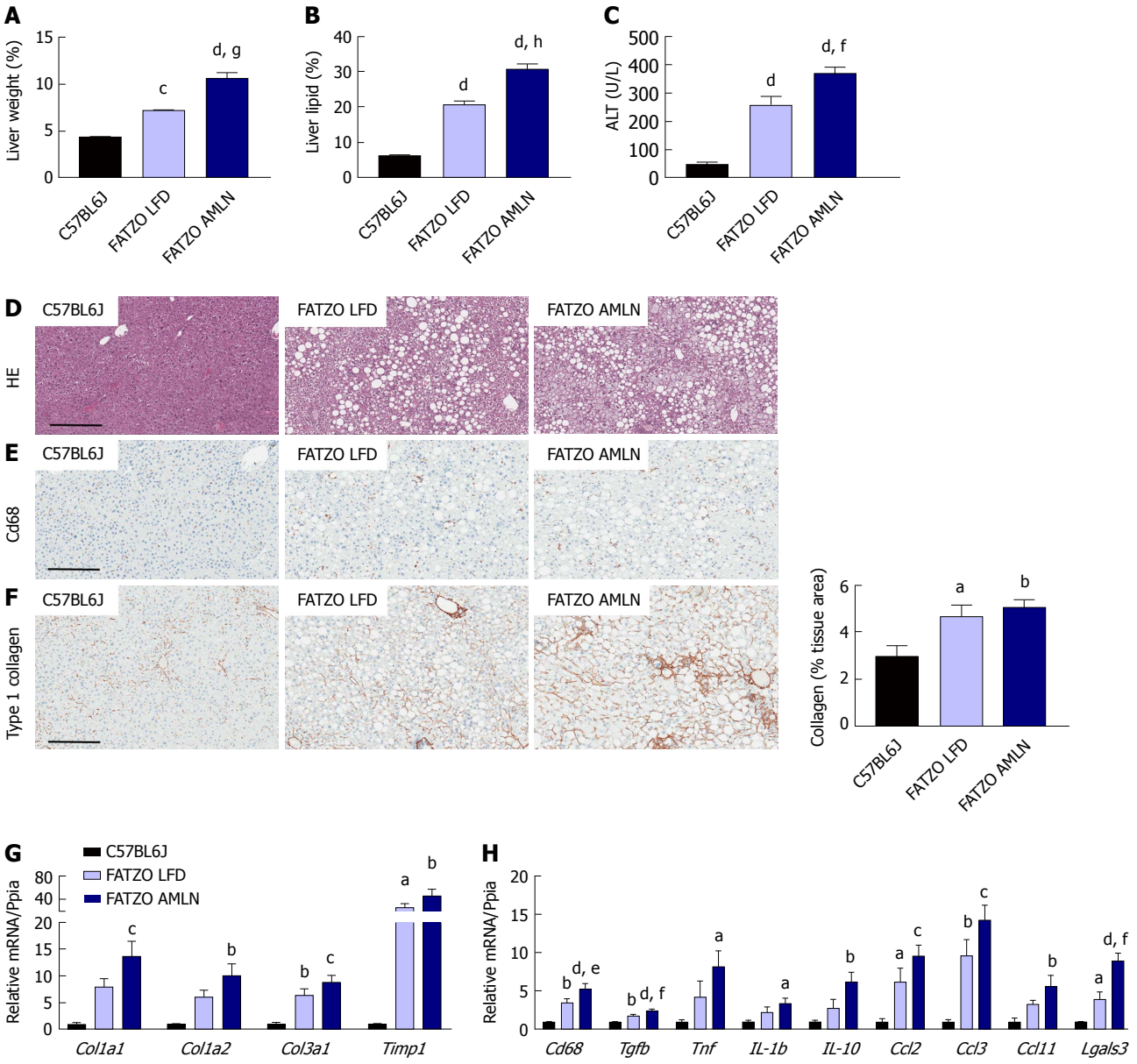

Figure 7 Comparison of metabolic and hepatic abnormalities associated with diet-induced nonalcoholic fatty liver disease/nonalcoholic steatohepatitis in FATZO mice. Liver weight (A), liver lipid (B), and plasma alanine aminotransferase (ALT) levels (C) of lean (C57BL6J) and FATZO mice maintained on control LFD (FATZO LFD) or AMLN diet (FATZO AMLN) for 12 wk; (D): Representative hematoxylin and eosin stained liver sections and quantification of percentage of liver area containing macrosteatosis; (E): Representative CD68-stained liver sections; (F): Representative collagen type 1 alpha 1 stained liver sections and quantification of collagen area; (G, H): Hepatic expression of genes associated with fibrosis and inflammation. $^{a}P \leqslant 0.05$, $^{b}P \leqslant 0.01$, $^{c}P \leqslant 0.001$, $^{d}P \leqslant 0.0001$ *vs* C57BL6J; $^{e}P \leqslant 0.05$, $^{f}P \leqslant 0.01$, $^{g}P \leqslant 0.001$, $^{h}P \leqslant 0.0001$ *vs* LFD. LFD: Low-fat diet.

FATZO mice on LFD and further induced by AMLN diet, indicating that the antioxidant response system was induced. Interestingly, when we quantified the expression levels of antioxidant enzymes that are collectively required for ROS detoxification, including superoxide dismustase 1 (*Sod1*), superoxide dismutase 2 (*Sod2*) and catalase (*Cat*), we detected unchanged or reduced hepatic expression in all diseased livers. *Sod1* mRNA was significantly reduced in both *ob/ob* LFD and *ob/ob* AMLN livers compared to lean controls (-25%, $P < 0.001$ for both; Figure 6A), while *Sod2* expression was significantly reduced in *ob/ob* AMLN livers compared to lean controls (-25%, $P < 0.05$; Figure 10A). All diseased livers displayed significantly reduced *Cat* expression compared to lean controls (-50%, $P < 0.0001$ for *ob/ob* LFD and AMLN *vs* lean controls; -20%, $P < 0.05$ for FATZO LFD and AMLN *vs* lean controls; Figure 10A). FATZO AMLN livers, however, did display significantly increased glutathione peroxidase (*Gpx1*) mRNA levels (+50%, $P < 0.01$ *vs* C57BL6J, Figure 10A).

Despite reduced (*ob/ob* mice) or unchanged (FATZO mice) *Sod1* and *Sod2* mRNA, there was a trend for increased hepatic superoxide dismutase activity for *ob/ob* and FATZO mice compared to lean controls ($P < 0.05$ *ob/ob* AMLN *vs* lean; Figure 10B). Catalase activity was increased approximately 2-fold in both FATZO LFD ($P < 0.001$) and FATZO AMLN livers ($P < 0.01$), but unchanged in *ob/ob* LFD and *ob/ob* AMLN

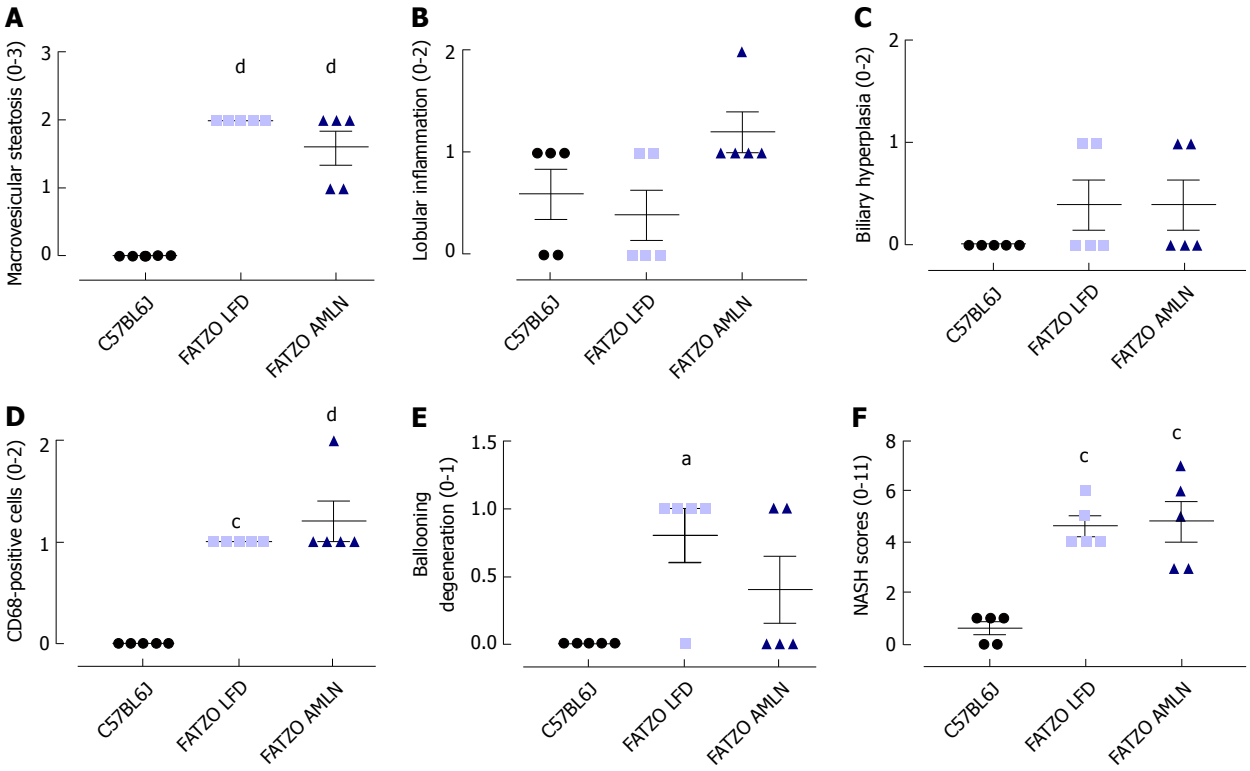

Figure 8 Histopathological scoring of FATZO mice. Individual grades of macrovesicular steatosis (A), lobular inflammation (B), biliary hyperplasia (C), CD68-positive cells (D) and ballooning degeneration. (E) Composite NASH scores. $^{a}P \leq 0.05$, $^{c}P \leq 0.001$, $^{d}P \leq 0.0001$ *vs* C57BL6J.

livers compared to lean controls (Figure 10C). We also detected increased catalase expression in liver sections from FATZO LFD and FATZO AMLN mice compared to lean controls (Figure 10D). Further, the ratio of hepatic catalase:SOD activity was reduced in *ob/ob* LFD mice and worsened by AMLN diet, but unchanged in FATZO animals compared to lean controls (Figure 10E). Hepatic 8-hydroxydeoxyguanosine (8-OHdG), a marker of oxidative DNA damage, tended to be higher in *ob/ob* LFD animals compared to both lean controls and FATZO LFD mice (Figure 10F). In *ob/ob* AMLN mice, hepatic 8-OHdG levels were significantly higher than both FATZO mice and lean controls (2.5-fold, $P < 0.01$ *vs* lean; Figure 10E). Additionally, we observed a negative correlation between catalase activity and hepatic 8-OHdG levels (Figure 10G). Taken together these data suggest that a reduced ability to manage ROS may be a key mechanism underlying the more severe liver phenotype observed in *ob/ob* AMLN mice.

DISCUSSION

The increasing health and economic burden and lack of FDA-approved therapies underscore the importance of appropriate pre-clinical models for NAFLD/NASH[22]. Surprisingly, only a handful of animal models are available that reflect human disease with respect to metabolic status and liver pathology[23,24]. These models are similar in that their genetic background predisposes to diet-induced NASH, and include the DIAMOND model[25], the *ob/ob* mouse[13,26], and the LDLR knockout mouse[27]. To a lesser extent, C57BL6J mice fed a high-fat (AMLN) diet will also develop NASH when given enough time (> 24 wk), but this model does not develop as advanced fibrosis[28,29]. Other reported models of liver disease do not develop liver inflammation, such as the APOE2 knock-in mouse[27], or lack metabolic context, such as the CCl_4 and MCDD models.

We report herein that both the leptin-deficient *ob/ob* mouse and hyperleptinemic FATZO mouse develop steatohepatitis within 12 wk of AMLN diet feeding. Despite similar levels of liver lipid and less severe hyperinsulinemia, *ob/ob* AMLN mice displayed a worse liver phenotype with increased inflammation and more advanced fibrosis relative to FATZO mice. Notably, hepatic expression of macrophage markers and related inflammatory chemokines were more prominently upregulated in *ob/ob* AMLN compared to FATZO AMLN mice, but were similar in *ob/ob* LFD and FATZO LFD animals, suggesting that the baseline inflammatory status and matrix deposition of the livers is similar in these models and that leptin deficiency *per se* does not predispose the liver to inflammation and fibrosis, but nonetheless may contribute to a proinflammatory, profibrotic phenotype upon dietary challenge.

While the precise pathophysiology of NASH remains to be fully determined, one aspect that has emerged in recent years is the role of mitochondrial (dys)function in hepatocytes associated with NAFLD/NASH. Evidence from human studies has recently emerged[8,30], however similar analyses in mouse models of NASH has not

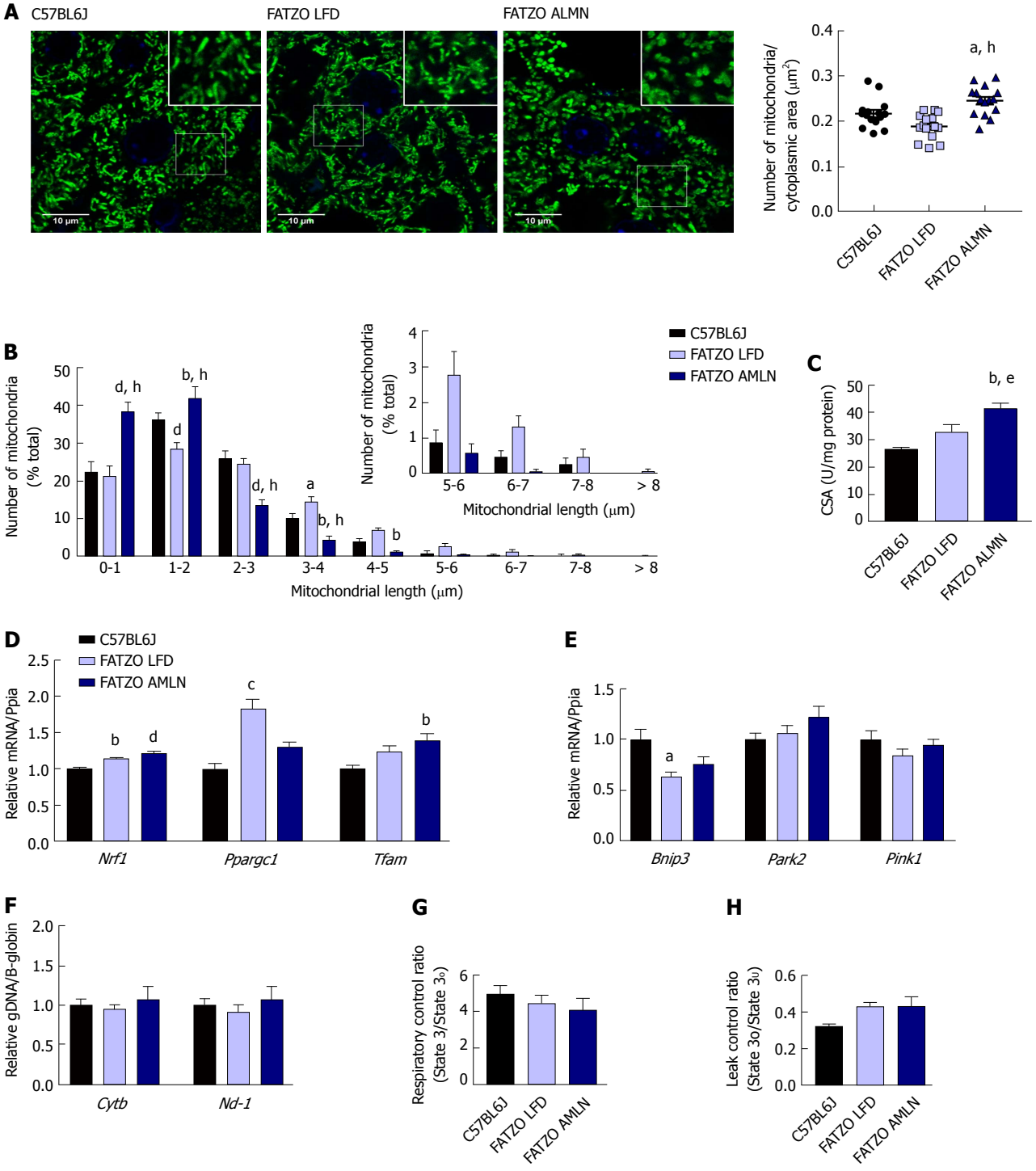

Figure 9 Mitochondrial content alterations in FATZO mice are associated with increased biogenesis and elevated proton leak. (A): Confocal images of HSP60 stained liver sections with quantification of mitochondrial number per cytoplasmic area. Scale bar = 10 μm; (B): Histogram depicting the number of mitochondria per binned mitochondrial length as a percentage of total mitochondria per cell; (C): Mitochondrial content measured by citrate synthase activity of isolated hepatic mitochondria; (D): Expression of hepatic mitochondrial biogenesis genes; (E): Relative hepatic expression of mitophagy-associated genes; (F): Quantification of mitochondrial genome-encoded *CytB* or *Nd1* relative to nuclear-encoded β- globin from total genomic DNA extracted from the liver; (G): Mitochondrial respiratory control ratio; (H): Mitochondrial leak control ratio. $^{a}P \leqslant 0.05$, $^{b}P \leqslant 0.01$, $^{c}P \leqslant 0.001$, $^{d}P \leqslant 0.0001$ *vs* C57BL6J; $^{e}P \leqslant 0.05$, $^{h}P \leqslant 0.0001$ *vs* LFD. LFD: Low-fat diet.

been reported. Multiple interconnected facets of mitochondrial biology including morphology, overall content (numbers and size), and respiratory capacity influence mitochondrial function. Our data show that *ob/ob* AMLN mice developed NASH associated with increased numbers of fragmented mitochondria with reduced respiratory capacity but without overt defects in mitochondrial membrane integrity or cristae structure. Similarly, FATZO AMLN mice displayed fragmented mitochondria with a trend for reduced respiratory control, but nonetheless better responded to oxidative damage and presented less overall fibrosis.

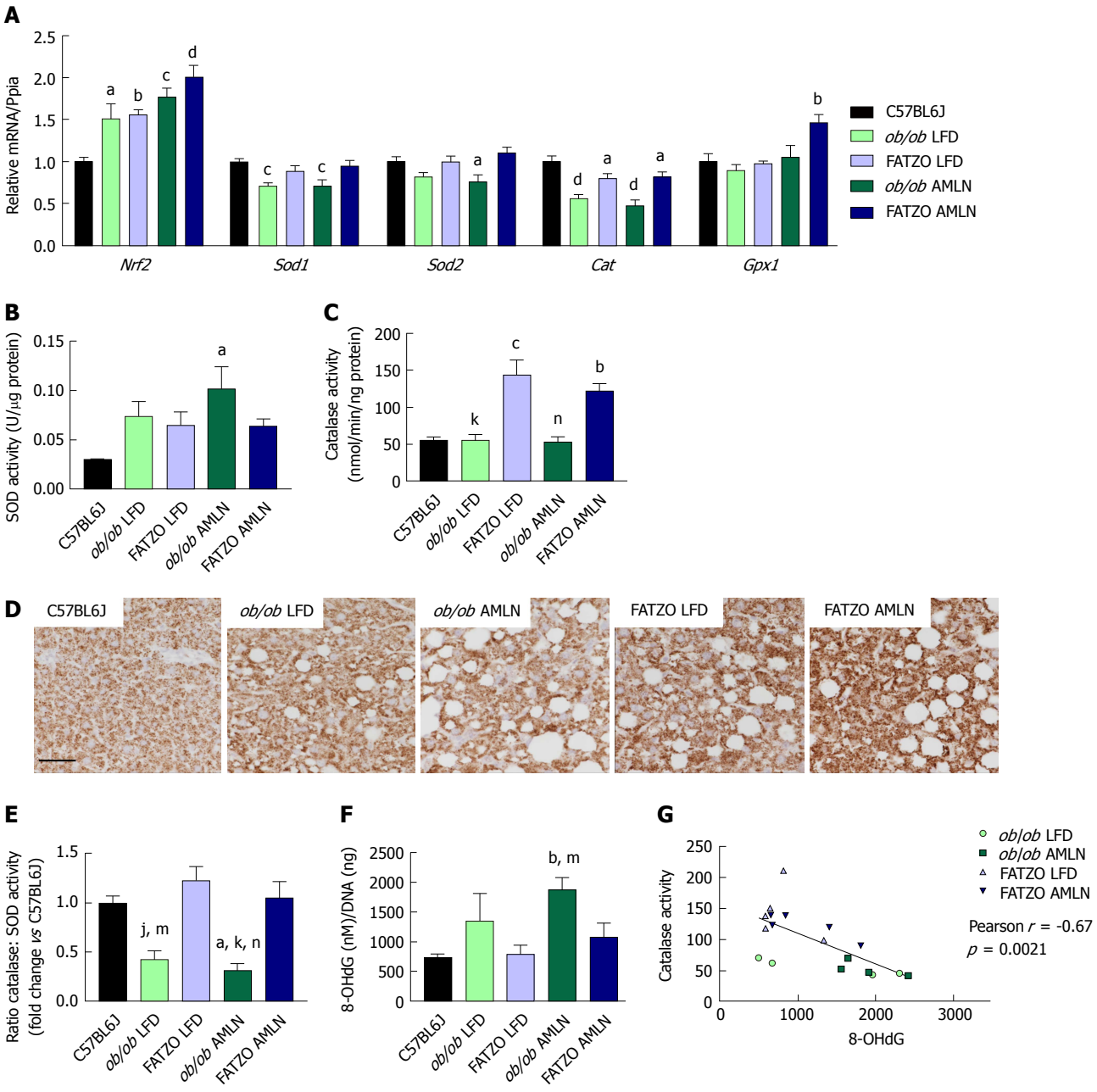

Figure 10 Hepatic oxidative stress is mitigated by increased catalase activity in FATZO but not *ob/ob* mice. (A): Expression of antioxidant genes *Nrf2*, *Sod1*, *Sod2*, *Cat* and *Gpx1* in *ob/ob* LFD, FATZO LFD, *ob/ob* AMLN and FATZO AMLN livers relative to lean controls. Superoxide dismutase activity (B) and catalase activity (C) in hepatic lysates from C57BL6J, *ob/ob* LFD, FATZO LFD, *ob/ob* AMLN and FATZO AMLN animals; (D): Representative images of catalase stained liver sections. Scale bar represents 100 μm; (E): Ratio of catalase: SOD activities; (F): Levels of 8-hydroxydeoxyguanosine (8-OHdG) in genomic DNA isolated from C57BL6J, *ob/ob* LFD, FATZO LFD, *ob/ob* AMLN and FATZO AMLN livers; (G): Pearson's correlation of catalase activity and 8-OHdG levels in *ob/ob* and FATZO livers. $^{a}P \leqslant 0.05$, $^{b}P \leqslant 0.01$, $^{c}P \leqslant 0.001$, $^{d}P \leqslant 0.0001$ *vs* C57BL6J; $^{j}P \leqslant 0.01$, $^{k}P \leqslant 0.001$, FATZO LFD; $^{m}P \leqslant 0.05$, $^{n}P \leqslant 0.01$, FATZO AMLN unless noted otherwise. LFD: Low-fat diet.

Mitochondrial morphology is appreciated to play an active role in regulating energy metabolism and cell death and can therefore influence NASH development at numerous stages[31,32]. Leptin has previously been shown to alter mitochondrial morphology and function. In primary mouse hepatocytes, leptin treatment induced mitochondrial fusion through induction of *Ppargc1a* and *Mfn1* and was associated with protection from high-glucose induced fatty acid accumulation[33]. Complementary work demonstrated that inhibition of mitochondrial fission reduced steatosis and development of NAFLD[34]. *Mfn1* and *Opa1* expression were significantly reduced in *ob/ob* mice when fed AMLN diet. Consistent with transcript levels, we observed smaller but more numerous mitochondria in both *ob/ob* AMLN and FATZO AMLN hepatocytes. Increased mitochondrial fragmentation and uncoupling have been proposed as adaptive mechanisms to reduce ROS levels and maintain energy balance by limiting ATP production in states of excess substrate supply which may explain the more fragmented, leaky mitochondria in *ob/ob* AMLN and FATZO AMLN livers.

Reduced mitochondrial function assessed by coupling efficiency and proton leak was also observed in both models; however, only *ob/ob* AMLN livers displayed significantly reduced mtDNA levels, similar to patients with NAFLD[35,36], which may affect other aspects of mitochondrial function including ATP generation and ROS production. Moreover, ROS itself may promote mtDNA mutation and degradation[37], leading to a feed-forward loop of continuous oxidative damage that leads to hepatocyte cell death, inflammation and fibrosis development. As such, targeting hepatic oxidative stress driven by chronic overnutrition could be an important therapeutic target for NASH prevention.

The capacity to manage oxidative stress was dissimilar between *ob/ob* and FATZO mice. Multiple antioxidant molecules within the cell are regulated by the transcription factor NRF2. While hepatic *Nrf2* expression was significantly upregulated in both *ob/ob* and FATZO livers, indicative of increased oxidative stress, oxidative DNA damage was only detected in *ob/ob* livers. Increased hepatic superoxide dismutase activity was detected in both *ob/ob* and FATZO animals, suggestive of elevated hydrogen peroxide in these livers, but concomitantly increased catalase activity and *Gpx1* expression was detected only in FATZO liver. Increased hepatic hydrogen peroxide levels have been reported for humans with NASH and correlated with catalase activity and oxidative DNA damage[8]. In line with these human studies, hepatic catalase activity was indeed negatively correlated with 8-OHdG levels.

In the clinic, single antioxidant therapy has shown mixed efficacy. Among these agents, vitamin E (despite its limited antioxidant efficacy) is the most investigated[38,39]. While the majority of studies showed improvements in select features, including steatosis, serum ALT and histopathology, none have demonstrated improvement in fibrosis, the key feature linked to disease progression[40]. Strategies to enhance antioxidant defenses are also being actively explored. One such target is NRF2, which can be activated by numerous natural products, including resveratrol and synthetic compounds[41]. Combination strategies that include the oxidant scavenging effects with an anti-fibrotic molecule such as the anti-galectin 3 drug GR-MD-02, currently in Phase 2 trials[42] may be informative.

In summary, we have described convenient mouse models of NAFLD/NASH that accurately reflect human disease context (obesity and insulin resistance) and liver pathology (steatosis, ballooning degeneration, inflammation and fibrosis). Additionally, both models appear to mimic reported aspects of mitochondrial phenotype in human NASH, including elevated mitochondrial numbers and increased proton leak. The unanticipated differences in disease severity may in part be due to an increased ability to manage oxidative stress in the FATZO mouse. These models may better predict therapeutic efficacy of putative NASH treatments in the clinic, particularly for agents targeting mitochondrial/oxidative pathways.

ARTICLE HIGHLIGHTS

Research background

Non-alcoholic steatohepatitis (NASH) is an unmet medical need with no approved therapies. Studies here characterize the hepatic phenotype of two different diet-induced mouse models of NASH with a focus on mitochondrial function and ability to regulate oxidative damage.

Research motivation

Emerging evidence from cross-sectional human studies suggests a role for mitochondrial function in the development of NASH. As the pathogenesis of NASH remains largely unknown it is imperative to characterize potential therapeutic agents in a relevant preclinical model.

Research objectives

The primary objective was to characterize NASH histopathology (*e.g.*, NASH activity score for steatosis, inflammation, ballooning and fibrosis) and function with a focus on mitochondrial biology and capacity to respond to oxidative stress. We contrast these endpoints in two distinct mouse strains (genetically obese Lep^{ob}/Lep^{ob} (*ob/ob*) and polygenic obesity-prone FATZO mice) on a previously validated NASH-inducing diet that is high in *trans*-fat, fructose and cholesterol (AMLN diet).

Research methods

Development of NASH was assessed using blinded qualitative (HE stained sections) and quantitative (% collagen-stained area) methods. Mitochondria were assessed via transmission electron micrography and immunofluorescent detection of HSP60. Mitochondrial function was assessed in primary hepatocytes using Seahorse. Activity of superoxide dismutase and catalase were measured from whole liver tissue homogenates. Candidate genes from total liver RNA were measured using quantitative PCR.

Research results

Both *ob/ob* and FATZO mice developed NASH with concomitant obesity and hyperinsulinemia when challenged with AMLN diet for 12 wk, and was associated with mitochondrial accumulation and reduced function. The degree of hepatic fibrosis, however, was markedly greater in *ob/ob* mice and was associated with increased activity of superoxide dismutase (SOD), whereas FATZO mice displayed increased catalase activity. Antioxidant capacity, reflected as the ratio of catalase: SOD activity, was significantly perturbed in *ob/ob* mice with diet-induced NASH.

Research conclusions

Both of these commonly available mouse models develop AMLN diet-induced NASH after 12 wk, associated with reduced mitochondrial function and perturbed morphology. The intrinsic capacity of the FATZO mice to increase antioxidant capacity in the face of impaired mitochondrial function/increased oxidative damage due to diet may be contributory towards the reduced level of fibrosis in that model.

Research perspectives

The AMLN mouse model of NASH is gaining widespread academic and industry acceptance as a translatable model of NASH. These studies extend previous observations in the model to highlight mitochondrial dysfunction thus confirming the model as relevant for prosecution of therapeutic agents targeting improvement in mitochondrial function for NASH. Furthermore, the contrasting fibrosis between *ob/ob* and FATZO mice implicates the capacity to adapt to oxidative damage as a key regulator of liver fibrosis in diet-induced NASH.

ACKNOWLEDGMENTS

We gratefully acknowledge the assistance of Sally Lee, Holly Koelkebeck, Wanda King, Kenesha Riley and Charles Brown (MedImmune, Gaithersburg, MD, United

States) for expert technical assistance with tissue processing and immunohistochemistry. We thank Lorenz Rognoni and Farzad Sekhavati (Definiens, Germany) for tissue image analysis. We also thank Donna Goldsteen, Krystal Nacel and the Laboratory Animal Resource staff (MedImmune, Gaithersburg, MD) for their assistance with animal husbandry and care.

REFERENCES

1 **Younossi ZM**, Blissett D, Blissett R, Henry L, Stepanova M, Younossi Y, Racila A, Hunt S, Beckerman R. The economic and clinical burden of nonalcoholic fatty liver disease in the United States and Europe. *Hepatology* 2016; **64**: 1577-1586 [PMID: 27543837 DOI: 10.1002/hep.28785]

2 **Younossi ZM**, Koenig AB, Abdelatif D, Fazel Y, Henry L, Wymer M. Global epidemiology of nonalcoholic fatty liver disease-Meta-analytic assessment of prevalence, incidence, and outcomes. *Hepatology* 2016; **64**: 73-84 [PMID: 26707365 DOI: 10.1002/hep.28431]

3 **Kabbany MN**, Conjeevaram Selvakumar PK, Watt K, Lopez R, Akras Z, Zein N, Carey W, Alkhouri N. Prevalence of Nonalcoholic Steatohepatitis-Associated Cirrhosis in the United States: An Analysis of National Health and Nutrition Examination Survey Data. *Am J Gastroenterol* 2017; **112**: 581-587 [PMID: 28195177 DOI: 10.1038/ajg.2017.5]

4 **Patterson RE**, Kalavalapalli S, Williams CM, Nautiyal M, Mathew JT, Martinez J, Reinhard MK, McDougall DJ, Rocca JR, Yost RA, Cusi K, Garrett TJ, Sunny NE. Lipotoxicity in steatohepatitis occurs despite an increase in tricarboxylic acid cycle activity. *Am J Physiol Endocrinol Metab* 2016; **310**: E484-E494 [PMID: 26814015 DOI: 10.1152/ajpendo.00492.2015]

5 **Satapati S**, Kucejova B, Duarte JA, Fletcher JA, Reynolds L, Sunny NE, He T, Nair LA, Livingston KA, Fu X, Merritt ME, Sherry AD, Malloy CR, Shelton JM, Lambert J, Parks EJ, Corbin I, Magnuson MA, Browning JD, Burgess SC. Mitochondrial metabolism mediates oxidative stress and inflammation in fatty liver. *J Clin Invest* 2016; **126**: 1605 [PMID: 27035816 DOI: 10.1172/JCI86695]

6 **Begriche K**, Massart J, Robin MA, Bonnet F, Fromenty B. Mitochondrial adaptations and dysfunctions in nonalcoholic fatty liver disease. *Hepatology* 2013; **58**: 1497-1507 [PMID: 23299992 DOI: 10.1002/hep.26226]

7 **Satapati S**, Sunny NE, Kucejova B, Fu X, He TT, Méndez-Lucas A, Shelton JM, Perales JC, Browning JD, Burgess SC. Elevated TCA cycle function in the pathology of diet-induced hepatic insulin resistance and fatty liver. *J Lipid Res* 2012; **53**: 1080-1092 [PMID: 22493093 DOI: 10.1194/jlr.M023382]

8 **Koliaki C**, Szendroedi J, Kaul K, Jelenik T, Nowotny P, Jankowiak F, Herder C, Carstensen M, Krausch M, Knoefel WT, Schlensak M, Roden M. Adaptation of hepatic mitochondrial function in humans with non-alcoholic fatty liver is lost in steatohepatitis. *Cell Metab* 2015; **21**: 739-746 [PMID: 25955209 DOI: 10.1016/j.cmet.2015.04.004]

9 **Auger C**, Alhasawi A, Contavadoo M, Appanna VD. Dysfunctional mitochondrial bioenergetics and the pathogenesis of hepatic disorders. *Front Cell Dev Biol* 2015; **3**: 40 [PMID: 26161384 DOI: 10.3389/fcell.2015.00040]

10 **Sunny NE**, Bril F, Cusi K. Mitochondrial Adaptation in Nonalcoholic Fatty Liver Disease: Novel Mechanisms and Treatment Strategies. *Trends Endocrinol Metab* 2017; **28**: 250-260 [PMID: 27986466 DOI: 10.1016/j.tem.2016.11.006]

11 **Gusdon AM**, Song KX, Qu S. Nonalcoholic Fatty liver disease: pathogenesis and therapeutics from a mitochondria-centric perspective. *Oxid Med Cell Longev* 2014; **2014**: 637027 [PMID: 25371775 DOI: 10.1155/2014/637027]

12 **Machado MV**, Michelotti GA, Xie G, Almeida Pereira T, Boursier J, Bohnic B, Guy CD, Diehl AM. Mouse models of diet-induced nonalcoholic steatohepatitis reproduce the heterogeneity of the human disease. *PLoS One* 2015; **10**: e0127991 [PMID: 26017539 DOI: 10.1371/journal.pone.0127991]

13 **Trevaskis JL**, Griffin PS, Wittmer C, Neuschwander-Tetri BA, Brunt EM, Dolman CS, Erickson MR, Napora J, Parkes DG, Roth JD. Glucagon-like peptide-1 receptor agonism improves metabolic, biochemical, and histopathological indices of nonalcoholic steatohepatitis in mice. *Am J Physiol Gastrointest Liver Physiol* 2012; **302**: G762-G772 [PMID: 22268099 DOI: 10.1152/ajpgi.00476.2011]

14 **Droz BA**, Sneed BL, Jackson CV, Zimmerman KM, Michael MD, Emmerson PJ, Coskun T, Peterson RG. Correlation of disease severity with body weight and high fat diet in the FATZO/Pco mouse. *PLoS One* 2017; **12**: e0179808 [PMID: 28640904 DOI: 10.1371/journal.pone.0179808]

15 **Peterson RG**, Jackson CV, Zimmerman KM, Alsina-Fernandez J, Michael MD, Emmerson PJ, Coskun T. Glucose dysregulation and response to common anti-diabetic agents in the FATZO/Pco mouse. *PLoS One* 2017; **12**: e0179856 [PMID: 28640857 DOI: 10.1371/journal.pone.0179856]

16 **Kleiner DE**, Brunt EM, Van Natta M, Behling C, Contos MJ, Cummings OW, Ferrell LD, Liu YC, Torbenson MS, Unalp-Arida A, Yeh M, McCullough AJ, Sanyal AJ; Nonalcoholic Steatohepatitis Clinical Research Network. Design and validation of a histological scoring system for nonalcoholic fatty liver disease. *Hepatology* 2005; **41**: 1313-1321 [PMID: 15915461 DOI: 10.1002/hep.20701]

17 **Alarcon C**, Boland BB, Uchizono Y, Moore PC, Peterson B, Rajan S, Rhodes OS, Noske AB, Haataja L, Arvan P, Marsh BJ, Austin J, Rhodes CJ. Pancreatic β-Cell Adaptive Plasticity in Obesity Increases Insulin Production but Adversely Affects Secretory Function. *Diabetes* 2016; **65**: 438-450 [PMID: 26307586 DOI: 10.2337/db15-0792]

18 **Kremer JR,** Mastronarde DN, McIntosh JR. Computer visualization of three-dimensional image data using IMOD. Journal of Structural Biology 1996; **116**: 71-76 [PMID: 8742726 DOI: 10.1006/jsbi.1996.0013]

19 **Boland BB**, Brown C Jr., Alarcon C, Demozay D, Grimsby JS, Rhodes CJ. β-Cell Control of Insulin Production During Starvation-Refeeding in Male Rats. *Endocrinology* 2018; **159**: 895-906 [PMID: 29244064 DOI: 10.1210/en.2017-03120]

20 **Glick D**, Zhang W, Beaton M, Marsboom G, Gruber M, Simon MC, Hart J, Dorn GW 2nd, Brady MJ, Macleod KF. BNip3 regulates mitochondrial function and lipid metabolism in the liver. *Mol Cell Biol* 2012; **32**: 2570-2584 [PMID: 22547685 DOI: 10.1128/MCB.00167-12]

21 **Chavin KD**, Yang S, Lin HZ, Chatham J, Chacko VP, Hoek JB, Walajtys-Rode E, Rashid A, Chen CH, Huang CC, Wu TC, Lane MD, Diehl AM. Obesity induces expression of uncoupling protein-2 in hepatocytes and promotes liver ATP depletion. *J Biol Chem* 1999; **274**: 5692-5700 [PMID: 10026188]

22 **Abdelmalek MF**. NAFLD: The clinical and economic burden of NAFLD: time to turn the tide. *Nat Rev Gastroenterol Hepatol* 2016; **13**: 685-686 [PMID: 27826139 DOI: 10.1038/nrgastro.2016.178]

23 **Hansen HH**, Feigh M, Veidal SS, Rigbolt KT, Vrang N, Fosgerau K. Mouse models of nonalcoholic steatohepatitis in preclinical drug development. *Drug Discov Today* 2017; **22**: 1707-1718 [PMID: 28687459 DOI: 10.1016/j.drudis.2017.06.007]

24 **Larter CZ**, Yeh MM. Animal models of NASH: getting both pathology and metabolic context right. *J Gastroenterol Hepatol* 2008; **23**: 1635-1648 [PMID: 18752564 DOI: 10.1111/j.1440-1746.2008.05543.x]

25 **Asgharpour A**, Cazanave SC, Pacana T, Seneshaw M, Vincent R, Banini BA, Kumar DP, Daita K, Min HK, Mirshahi F, Bedossa P, Sun X, Hoshida Y, Koduru SV, Contaifer D Jr, Warncke UO, Wijesinghe DS, Sanyal AJ. A diet-induced animal model of non-alcoholic fatty liver disease and hepatocellular cancer. *J Hepatol* 2016; **65**: 579-588 [PMID: 27261415 DOI: 10.1016/j.jhep.2016.05.005]

26 **Clapper JR**, Hendricks MD, Gu G, Wittmer C, Dolman CS, Herich J, Athanacio J, Villescaz C, Ghosh SS, Heilig JS, Lowe C, Roth JD.

Diet-induced mouse model of fatty liver disease and nonalcoholic steatohepatitis reflecting clinical disease progression and methods of assessment. *Am J Physiol Gastrointest Liver Physiol* 2013; **305**: G483-G495 [PMID: 23886860 DOI: 10.1152/ajpgi.00079.2013]

27 **Bieghs V**, Van Gorp PJ, Wouters K, Hendrikx T, Gijbels MJ, van Bilsen M, Bakker J, Binder CJ, Lütjohann D, Staels B, Hofker MH, Shiri-Sverdlov R. LDL receptor knock-out mice are a physiological model particularly vulnerable to study the onset of inflammation in non-alcoholic fatty liver disease. *PLoS One* 2012; **7**: e30668 [PMID: 22295101 DOI: 10.1371/journal.pone.0030668]

28 **Liedtke C**, Luedde T, Sauerbruch T, Scholten D, Streetz K, Tacke F, Tolba R, Trautwein C, Trebicka J, Weiskirchen R. Experimental liver fibrosis research: update on animal models, legal issues and translational aspects. *Fibrogenesis Tissue Repair* 2013; **6**: 19 [PMID: 24274743 DOI: 10.1186/1755-1536-6-19]

29 **Kristiansen MN**, Veidal SS, Rigbolt KT, Tølbøl KS, Roth JD, Jelsing J, Vrang N, Feigh M. Obese diet-induced mouse models of nonalcoholic steatohepatitis-tracking disease by liver biopsy. *World J Hepatol* 2016; **8**: 673-684 [PMID: 27326314 DOI: 10.4254/wjh.v8.i16.673]

30 **Hyötyläinen T**, Jerby L, Petäjä EM, Mattila I, Jäntti S, Auvinen P, Gastaldelli A, Yki-Järvinen H, Ruppin E, Orešič M. Genome-scale study reveals reduced metabolic adaptability in patients with non-alcoholic fatty liver disease. *Nat Commun* 2016; **7**: 8994 [PMID: 26839171 DOI: 10.1038/ncomms9994]

31 **Westermann B**. Mitochondrial fusion and fission in cell life and death. *Nat Rev Mol Cell Biol* 2010; **11**: 872-884 [PMID: 21102612 DOI: 10.1038/nrm3013]

32 **Wai T**, Langer T. Mitochondrial Dynamics and Metabolic Regulation. *Trends Endocrinol Metab* 2016; **27**: 105-117 [PMID: 26754340 DOI: 10.1016/j.tem.2015.12.001]

33 **Hsu WH**, Lee BH, Pan TM. Leptin-induced mitochondrial fusion mediates hepatic lipid accumulation. *Int J Obes* (Lond) 2015; **39**: 1750-1756 [PMID: 26119995 DOI: 10.1038/ijo.2015.120]

34 **Galloway CA**, Lee H, Brookes PS, Yoon Y. Decreasing mitochondrial fission alleviates hepatic steatosis in a murine model of nonalcoholic fatty liver disease. *Am J Physiol Gastrointest Liver Physiol* 2014; **307**: G632-G641 [PMID: 25080922 DOI: 10.1152/ajpgi.00182.2014]

35 **Sookoian S**, Rosselli MS, Gemma C, Burgueño AL, Fernández Gianotti T, Castaño GO, Pirola CJ. Epigenetic regulation of insulin resistance in nonalcoholic fatty liver disease: impact of liver methylation of the peroxisome proliferator-activated receptor γ coactivator 1α promoter. *Hepatology* 2010; **52**: 1992-2000 [PMID: 20890895 DOI: 10.1002/hep.23927]

36 **Sookoian S**, Flichman D, Scian R, Rohr C, Dopazo H, Gianotti TF, Martino JS, Castaño GO, Pirola CJ. Mitochondrial genome architecture in non-alcoholic fatty liver disease. *J Pathol* 2016; **240**: 437-449 [PMID: 27577682 DOI: 10.1002/path.4803]

37 **Shokolenko I**, Venediktova N, Bochkareva A, Wilson GL, Alexeyev MF. Oxidative stress induces degradation of mitochondrial DNA. *Nucleic Acids Res* 2009; **37**: 2539-2548 [PMID: 19264794 DOI: 10.1093/nar/gkp100]

38 **Al-Busafi SA**, Bhat M, Wong P, Ghali P, Deschenes M. Antioxidant therapy in nonalcoholic steatohepatitis. *Hepat Res Treat* 2012; **2012**: 947575 [PMID: 23227320 DOI: 10.1155/2012/947575]

39 **Sanyal AJ**, Chalasani N, Kowdley KV, McCullough A, Diehl AM, Bass NM, Neuschwander-Tetri BA, Lavine JE, Tonascia J, Unalp A, Van Natta M, Clark J, Brunt EM, Kleiner DE, Hoofnagle JH, Robuck PR; NASH CRN. Pioglitazone, vitamin E, or placebo for nonalcoholic steatohepatitis. *N Engl J Med* 2010; **362**: 1675-1685 [PMID: 20427778 DOI: 10.1056/NEJMoa0907929]

40 **Hagström H**, Nasr P, Ekstedt M, Hammar U, Stål P, Hultcrantz R, Kechagias S. Fibrosis stage but not NASH predicts mortality and time to development of severe liver disease in biopsy-proven NAFLD. *J Hepatol* 2017; **67**: 1265-1273 [PMID: 28803953 DOI: 10.1016/j.jhep.2017.07.027]

41 **Musso G**, Cassader M, Gambino R. Non-alcoholic steatohepatitis: emerging molecular targets and therapeutic strategies. *Nat Rev Drug Discov* 2016; **15**: 249-274 [PMID: 26794269 DOI: 10.1038/nrd.2015.3]

42 **Harrison SA**, Marri SR, Chalasani N, Kohli R, Aronstein W, Thompson GA, Irish W, Miles MV, Xanthakos SA, Lawitz E, Noureddin M, Schiano TD, Siddiqui M, Sanyal A, Neuschwander-Tetri BA, Traber PG. Randomised clinical study: GR-MD-02, a galectin-3 inhibitor, vs. placebo in patients having non-alcoholic steatohepatitis with advanced fibrosis. *Aliment Pharmacol Ther* 2016; **44**: 1183-1198 [PMID: 27778367 DOI: 10.1111/apt.13816]

P- Reviewer: Garcia-Fernandez MI, Novo E, Streba LAM
S- Editor: Ma YJ **L- Editor**: A **E- Editor**: Huang Y

Published by **Baishideng Publishing Group Inc**
7901 Stoneridge Drive, Suite 501, Pleasanton, CA 94588, USA
Telephone: +1-925-223-8242
Fax: +1-925-223-8243
E-mail: bpgoffice@wjgnet.com
Help Desk: http://www.f6publishing.com/helpdesk
http://www.wjgnet.com

ISSN 1007-9327